Decreased non-neurogenic acetylcholine in bone marrow triggers age-related defective stem/progenitor cell homing

Takayuki Morikawa[1], Shinya Fujita[1], Yuki Sugiura [2,3], Shinpei Tamaki[1], Miho Haraguchi[1,4], Kohei Shiroshita [1], Shintaro Watanuki[1,5], Hiroshi Kobayashi [1,5], Hikari Kanai-Sudo[1], Yoshiko Naito[6], Noriyo Hayakawa[7], Tomomi Matsuura[6], Takako Hishiki [8], Minoru Matsui[9], Masato Tsutsui[10], Makoto Suematsu[3,7] & Keiyo Takubo [1,5,11] ✉

Age-related decline in the ability of bone marrow (BM) to recruit transplanted hematopoietic stem and progenitor cells (HSPCs) limits the potential of HSPC-based medicine. Using in vivo imaging and manipulation combined with integrative metabolomic analyses, we show that, with aging, degradation of non-neurogenic acetylcholine disrupts the local Chrm5-eNOS-nitric oxide signaling, reducing arterial dilation and decreasing both BM blood flow and sinusoidal wall shear stress. Consequently, aging BM microenvironment impairs transendothelial migration of transplanted HSPCs, and their BM homing efficiency is reduced, mediated by decreased activation of Piezo1. Notably, pharmacological activation of Piezo1 improves HSPC homing efficiency and post-transplant survival of aged recipients. These findings suggest that age-related dysregulation of local arteries leads to impaired HSPC homing to BM by decreasing shear stress. Modulation of these mechanisms may improve the efficacy and safety of clinical transplantation in elderly patients.

The hematopoietic system relies on hematopoietic stem cells (HSCs), hematopoietic progenitor cells (HPCs), and the bone marrow (BM) niche to maintain coordinated production of blood cell lineages throughout adult life[1–4]. While HSCs can generate HPCs in the BM niche, both also migrate to the periphery to enhance peripheral immune defense and subsequently home back to the BM[5–7]. Although homing of HSCs and HPCs (HSPC) is a physiological process, efficient homing of transplanted HSPCs is also a critical step for successful HSC transplantation (HSCT). A notable age-related dysfunction of the hematopoietic system is the decline in HSPC homing to irradiated BM, yet the underlying mechanisms remain poorly understood[8]. It is also unclear how steady-state homing of circulating HSPCs to the BM niche changes with age. To improve the outcome of HSCT followed by various intensities of preconditioning in elderly patients with age-related or refractory hematological diseases, it is essential to study the age-related decline in HSPC homing efficiency. Understanding its mechanisms involved may help to improve clinical care of these patients.

[1]Department of Stem Cell Biology, National Institute of Global Health and Medicine, Japan Institute for Health Security, Tokyo, Japan. [2]Multiomics Platform, Center for Cancer Immunotherapy and Immunobiology, Kyoto University Graduate School of Medicine, Kyoto, Japan. [3]WPI-Bio2Q Research Center, Keio University, Tokyo, Japan. [4]Kanagawa Institute of Industrial Science and Technology (KISTEC), Kawasaki, Kanagawa, Japan. [5]Department of Cell Fate Biology and Stem Cell Medicine, Tohoku University Graduate School of Medicine, Sendai, Miyagi, Japan. [6]Clinical Translational Research Center, Keio University Hospital, Tokyo, Japan. [7]Central Institute for Experimental Medicine and Life Science, Kawasaki, Kanagawa, Japan. [8]Department of Health Chemistry, Showa Pharmaceutical University, Machida, Tokyo, Japan. [9]Yokokawa Ladies Clinic, Tokyo, Japan. [10]Department of Pharmacology, Graduate School of Medicine, University of the Ryukyus, Okinawa, Japan. [11]Japan Agency for Medical Research and Development (AMED), Core Research for Evolutional Science and Technology (CREST), Tokyo, Japan. ✉e-mail: keiyot@gmail.com

The BM vasculature originates in the nutrient arteries that penetrate the bone and connect via arterioles to dilated sinusoidal vessels[9]. Homing of circulating HSPCs occurs through the sinusoidal endothelium[10–12]. HSPC homing to BM is somewhat similar to leukocyte homing to inflammatory tissues, and involves rolling, adhesion to the endothelial lumen, and transendothelial migration (TEM)[13–15]. Factors such as C-X-C motif chemokine ligand 12 (CXCL12), prostaglandin E2, sphingosine 1-phosphate, and osteopontin are derived from BM niche cells and act directly on HSPCs to promote homing to BM[16–20]. Downstream from these factors, integrin-, selectin- or CD44-mediated cell rolling or adhesion and small G-protein-mediated cell motility and cytoskeletal remodeling occur, and finally, HSPCs arrive in BM[21–31].

In addition to ligand-induced mechanisms, differentiated leukocyte TEM is facilitated by a physical factor, shear stress[32]. Recently, the endothelial mechano-gated ion channel, Piezo1, was reported to be required for leukocyte TEM by sensing wall shear stress and inducing calcium entry into endothelial cells[33]. In BM, there is a certain range of shear stress in the sinusoidal vessel wall shear where HSPC homing occurs[15]. However, the regulatory mechanisms of BM hemodynamics including sinusoidal shear stress, its contribution to HSPC homing to BM, and its significance in the age-related decline in homing efficiency are not known.

In this study, we used rapid fixation-based metabolomic analysis and in vivo imaging and manipulation to investigate mechanisms of defective HSPC homing in aged BM. Here we identify the molecular basis for the age-related decline in HSPC homing to BM and propose methods to ameliorate it. Our data indicate that increased degradation of non-neurogenic acetylcholine (ACh) in aged BM decreases nitric oxide (NO)-mediated perfusion, reduces wall shear stress, and suppresses activation of Piezo1, thereby reducing the homing efficiency of transplanted HSPCs. Pharmacological activation of Piezo1 improves homing efficiency and survival in aged mice, suggesting that targeting shear stress and related mechanisms may improve clinical HSCT in elderly patients.

Results

HSPCs in old BM show a metabolic state consistent with hypoperfusion

To identify changes in the aged BM environment, including age-related decline in the ability to recruit transplanted cells, we investigated the metabolic state of HSPCs, which is sensitive to environmental changes. For this purpose, we used capillary electrophoresis-mass spectrometry (CE-MS) to perform metabolomic analysis (Fig. 1a, Supplementary Fig. 1a, Supplementary Table 1). Hierarchical cluster analysis based on age-related changes in metabolite concentrations revealed two major clusters, one composed of up-regulated metabolites and the other of down-regulated metabolites during aging (Supplementary Fig. 1b). These data suggest that aging of the BM microenvironment induces similar metabolic effects in both HSCs and MPP1.

Among these metabolite changes, several TCA cycle intermediates decreased in HSCs with aging (Fig. 1b). For example, levels of citrate and isocitrate in HSCs were lower in old mice than in young or middle-aged mice, and other TCA cycle intermediates tended to decrease with age (Fig. 1c, Supplementary Fig. c). Age-related decreases in TCA cycle metabolites were also observed in MPP1 (Fig. 1d, Supplementary Fig. 1d). An explanation for these changes is that increased consumption of TCA intermediates occurs in aged HSPCs. The TCA cycle drives oxidative phosphorylation to produce the energy currency, ATP[34]. In our experiments, however, there was no increase in ATP concentration or its breakdown products with aging (Fig. 1e), nor was there an increase in energy charge, a parameter that reflects ATP production and utilization[35] (Fig. 1f). So, we considered another possibility.

Hierarchical clustering analysis of changes in metabolite levels in HSCs during aging revealed a decrease in many amino acids (Fig. 1b).

We compared intracellular amino acid levels between young and old HSCs. The total amount of amino acids in old HSCs was about 20% of that in young HSCs, except for two acidic amino acids. Similarly, levels of 80% of the amino acids were lower in old MPP1s than those in young MPP1s (Fig. 1g, Supplementary Table 1). In contrast, there were no significant age-related changes in the total amount of intracellular protein in HSPCs (Fig. 1h), suggesting that the decrease in amino acids in HSPCs with aging is not due to changes in protein production or degradation. These results suggest that the age-related decline in TCA intermediates and amino acids is likely due to an insufficient supply of these metabolites or their metabolic precursors. Consistent with this, total levels of glycolytic intermediates were lower in old HSPCs than in young HSPCs (Fig. 1i). These metabolic profiles of HSPCs suggest a reduction of metabolite supply by blood flow to the aged BM niche.

Blood flow in the HSPC niche decreases during aging

To directly investigate age-related changes in blood flow in the HSPC niche, we used Evi1-IRES-GFP knockin (Evi1-GFP) mice[36], with labeled HSCs and some MPPs, to visualize HSPCs and their surrounding microenvironment (Supplementary Fig. 2a). GFP[high] frequency in HSPCs and other BM fractions of old Evi1-GFP mice was comparable to that of young mice (Supplementary Fig. 2b). By intravital imaging using multiphoton laser microscopy, we observed sinusoids around Evi1-GFP[high] HSPCs in BM of both young and old mice (Fig. 2a, b).

First, we measured the distance between HSPCs and sinusoids in young and old BMs to account for the possibility of reduced metabolite delivery due to topological changes in HSPCs and sinusoids. However, we did not find distance changes or changes in GFP[high] cell distribution with aging (Supplementary Fig. 2c). Next, to assess whether the decrease in metabolites in HSPCs with age was due to decreased exchange vessel (sinusoid) density in the aged HSC niche, we compared it in young and old niches. However, sinusoidal density in aged HSC niches was not significantly different from that in young niches (Fig. 2c, Supplementary Fig. 2d). Therefore, considering the possibility of altered BM microcirculation, we compared blood flow between young, middle-aged, and old HSC niches using intravital imaging[15,37]. Intravital staining with Alexa Fluor 633 (AF633) and acetylated low-density lipoproteins (AcLDLs) were used to identify arteries and sinusoids in BM of living Evi1-GFP mice, respectively (Supplementary Fig. 2e)[38]. While diameter and intravascular volume of sinusoids were unchanged, arterial diameter and flux decreased with age, and the velocity, flux, shear rate, and shear stress of sinusoids around old HSPCs were lower than those around young HSPCs (Fig. 2c–e). These data suggest that perfusion is reduced in aged HSC niches, as suggested by metabolic changes in HSPCs with aging.

Old BM tissue exhibits a metabolic profile associated with decreased NO signaling

Metabolomic analysis suggested a similar metabolic deficiency in both HSCs and MPP1 (Fig. 1). In addition, because a reduction in overall BM blood flow was observed (Fig. 2), we hypothesized that metabolic changes were occurring throughout the BM, and we sought to identify these changes. To evaluate mechanisms underlying the age-related decline in BM perfusion, we performed a metabolomic analysis of whole BM tissue samples of different ages using CE-MS (Fig. 3a, Supplementary Table 2). Although 60% of detected metabolites were not significantly different between young and old BM samples, most other metabolites were decreased in the aged group and the number of decreased metabolites in BM tissues was greater in old mice than in middle-aged mice (Fig. 3b). Hierarchical cluster analysis revealed a cluster of metabolites that decreased with age in both HSPCs and whole BM tissues, and this cluster contained many amino acids (Fig. 3c). In particular, levels of many amino acids detected (11 decreased and 8 unchanged) were lower in old BM than in young BM (Supplementary Fig. 3a). To investigate whether these decreases in amino

acids were due to changes in serum amino acids, we measured serum amino acid concentrations in young and old mice by CE-MS (Supplementary Table 3). Unlike BM, the concentrations of almost all serum amino acids tended to be higher (7 increased and 12 unchanged) in old mice than in young mice (Supplementary Fig. 3b), indicating that the decrease in BM amino acids during aging is independent of changes in serum amino acid concentrations. As in HSPCs, certain TCA intermediates, such as *cis*-aconitate and α-KG decreased in whole BM tissue during aging, and other TCA cycle metabolites tended to be lower in old BM tissue than in young BM tissue (Supplementary Fig. 3c). These findings support the possibility that blood flow, which transports these metabolites to BM, decreases with age. To identify factors that induce

age-related reductions in BM blood flow, we performed Ingenuity Pathway Analysis (IPA) using young mice as a baseline, and found downregulation of the endothelial nitric oxide (NO) synthase (eNOS) signaling pathway[39] during aging (Fig. 3d). On the other hand, the IPA using middle-aged mice as the baseline showed slight downregulation in eNOS signaling pathway activity from middle-aged to old (Z-score, −0.447). Further IPA analysis showed that of the pathways identified as significantly variable during the aging process, only the eNOS signaling pathway decreased with age (Fig. 3e, Supplementary Fig. 3d). In particular, levels of arginine and ACh, the natural substrate and activator of NO production, respectively, decreased with age (Fig. 3f). To verify whether ACh induces NO production in vivo, calvarial BM was treated
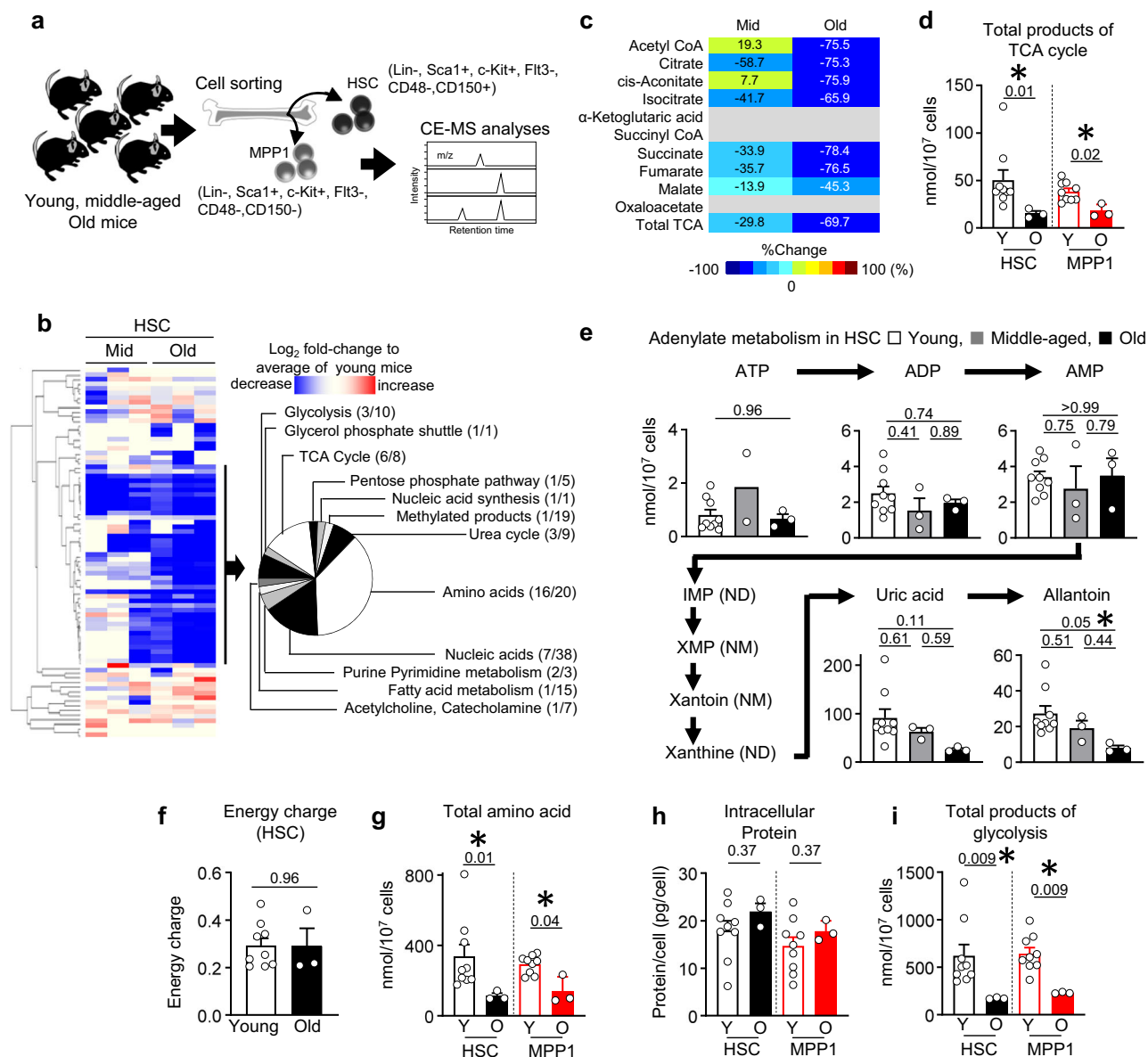

Fig. 1 | Metabolic profiling of old HSPCs suggests a low-nutrition state.
a Metabolomic profiling of HSCs and MPP1. **b** Cluster analysis of metabolites that increased or decreased during HSC aging. The pie chart shows classification of metabolites that decreased during aging. (young, $n = 9$; middle-aged, $n = 3$; old, $n = 3$ biological replicates) **c** Age-related changes of TCA cycle metabolites in HSCs. Numbers in the chart indicate rates of changes from young to middle-aged and old mice. Gray boxes indicate unmeasured or undetected metabolites (young, $n = 9$; middle-aged, $n = 3$; old, $n = 3$ biological replicates). **d** Total amounts of TCA cycle metabolites in HSCs or MPP1s from young (Y) and old (O) mice (young, $n = 9$; old,

$n = 3$ biological replicates). **e** Levels of ATP and related metabolites in HSCs in various ages (young, $n = 9$; middle-aged, $n = 3$; old, $n = 3$ biological replicates). **f** Energy charge in HSC (young, $n = 9$; old, $n = 3$ biological replicates), ND, not detected; NM, not measured. **g–i** Total amounts of amino acids (**g**), protein amounts (**h**), and total amounts of glycolytic metabolites (**i**) in HSCs and MPP1s from young (Y) and old (O) mice. (young, $n = 9$; old, $n = 3$ biological replicates). Values are mean ± SEM (**d–i**). **d** and **f–i** Two-sided Mann–Whitney U test. **e** One-way ANOVA with Tukey–Kramer test. *$p < 0.05$. Source data are provided with this paper.
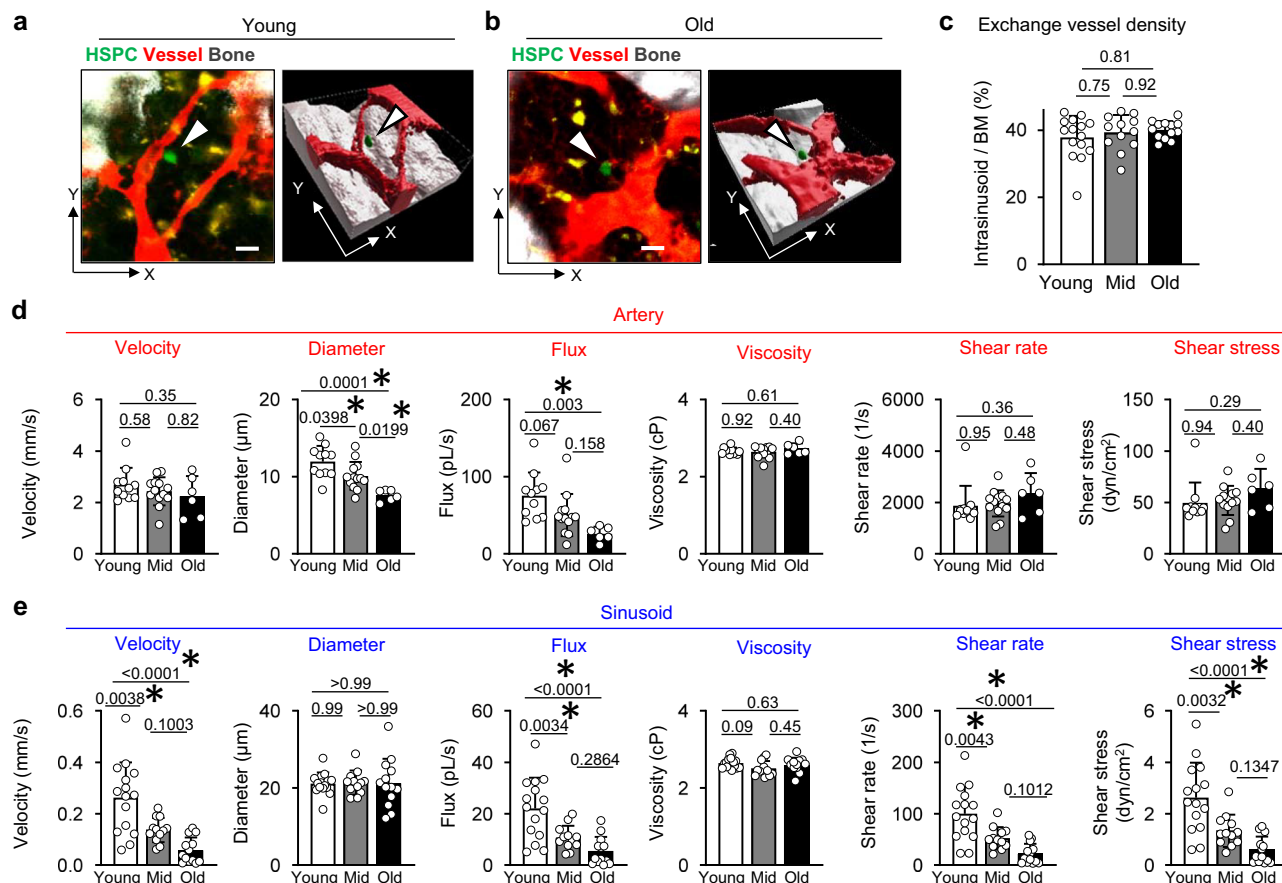
Fig. 2 | **Blood flow in the HSPC niche decreases during aging. a, b** Intravital BM imaging of Evi1^{high} HSPCs and adjacent blood vessels in young (**a**) or old (**b**) Evi1-GFP mice before (left) and after (right) 3D rendering. Arrowhead indicates Evi1^{high} HSPC. Bar = 10 μm. **c** Percentage of intrasinusoidal volume in BM (young, $n = 15$; middle-aged, $n = 12$, old, $n = 13$ biological replicates). **d, e** Hemodynamic parameters of artery (**d**) or sinusoid (**e**) in BM of young (artery, $n = 11$; sinusoid, $n = 15$ biological replicates), middle-aged (artery, $n = 13$; sinusoid, $n = 12$ biological replicates), and old mice (artery, $n = 6$; sinusoid, $n = 13$ biological replicates). Values are mean ± SD. One-way ANOVA with Tukey–Kramer test. *$p < 0.05$. Source data are provided with this paper.

with carbamylcholine, an agonist of AChR. In BM, NO production was significantly observed, especially in arteries (Supplementary Fig. 4a). Downstream of the eNOS enzymatic reaction, guanine triphosphate (GTP), the substrate of soluble guanylate cyclase (sGC) activated by NO, accumulated with age. In addition, NO concentration in old BM was lower than that in young BM (Fig. 3g). Collectively, these results suggest that reduced NO signal is a potential mechanism of the age-related decline in BM perfusion.

The age-related decline in BM amino acid concentrations may involve mechanisms beyond reduced blood flow. For example, aging has been reported to induce a myeloid differentiation bias in HSCs after transplantation[40–42]. To investigate whether this bias is reflected under steady-state metabolite changes, we analyzed the proportion of myeloid cells in BM of young and aged mice. The proportion of myeloid cells remained constant at ~50% in both age groups. Furthermore, metabolomic analysis of isolated myeloid cells showed no significant age-related changes in amino acid or other metabolite concentrations (Supplementary Fig. 4b–e, Supplementary Table 4). Therefore, we investigated the impact of changes in blood flow as the primary factor.

Degradation of non-neurogenic ACh increases in old BM

ACh is provided by neuronal and non-neuronal cells expressing choline acetyltransferase (ChAT), an enzyme catalyzing the essential step of ACh synthesis[43]. We investigated ChAT localization and its changes by using ChAT (BAC)-eGFP (ChAT[BAC]-eGFP) transgenic mice[44]. First, we immunohistochemically analyzed BM of young and old ChAT[BAC]-eGFP mice. ChAT[+] blood cell-like round cells were observed in both young

and old BMs, and their frequency and localization did not change with age (Fig. 4a, Supplementary Fig. 4f, g). Flow cytometric analysis revealed that, consistent with previous reports[45,46], B cells were the major population of ChAT-expressing hematopoietic cells in young BM (Supplementary Fig. 4h, i). Old BM had a higher proportion of T cells among ChAT-expressing cells than young BM, but B cells remained the largest population of ChAT-expressing cells. These results suggest that ACh is mainly produced by B cells in young BM, as reported, and additionally by T cells in old BM.

Hydrolysis of ACh by its esterase (AChE) is a crucial process in ACh metabolism that prevents overstimulation of ACh-receiving cells, including cholinergic neurons in nerve ganglia[47]. To investigate mechanisms that explain the age-related ACh reduction in BM, we compared protein levels and enzymatic activity of AChE in young and old BM. Western blot analysis showed higher levels of AChE in old BM compared to young BM (Fig. 4b, c); and enzymatic activity of AChE also increased with age (Fig. 4d). Next, to determine the major source of AChE in young and old BM, we analyzed single-cell RNA-sequencing (scRNA-seq) data of Tabula Muris Senis (https://tabula-muris-senis.ds.czbiohub.org) and GSE255019. Uniform manifold approximation and projection (UMAP) of scRNA-seq data for whole BM cells identified AChE expression in both young and old BM (Supplementary Fig. 5a, c). AChE expression was detected in immature B cells, granulocytopoietic cells, erythroblasts, granulocytes, hematopoietic precursor cells, megakaryocyte precursor cell (MkP) and erythroid (Supplementary Fig. 5b, d). In particular, immature B cells, MkP and erythroid expressing AChE increased with age, and AChE-positive granulocytopoietic
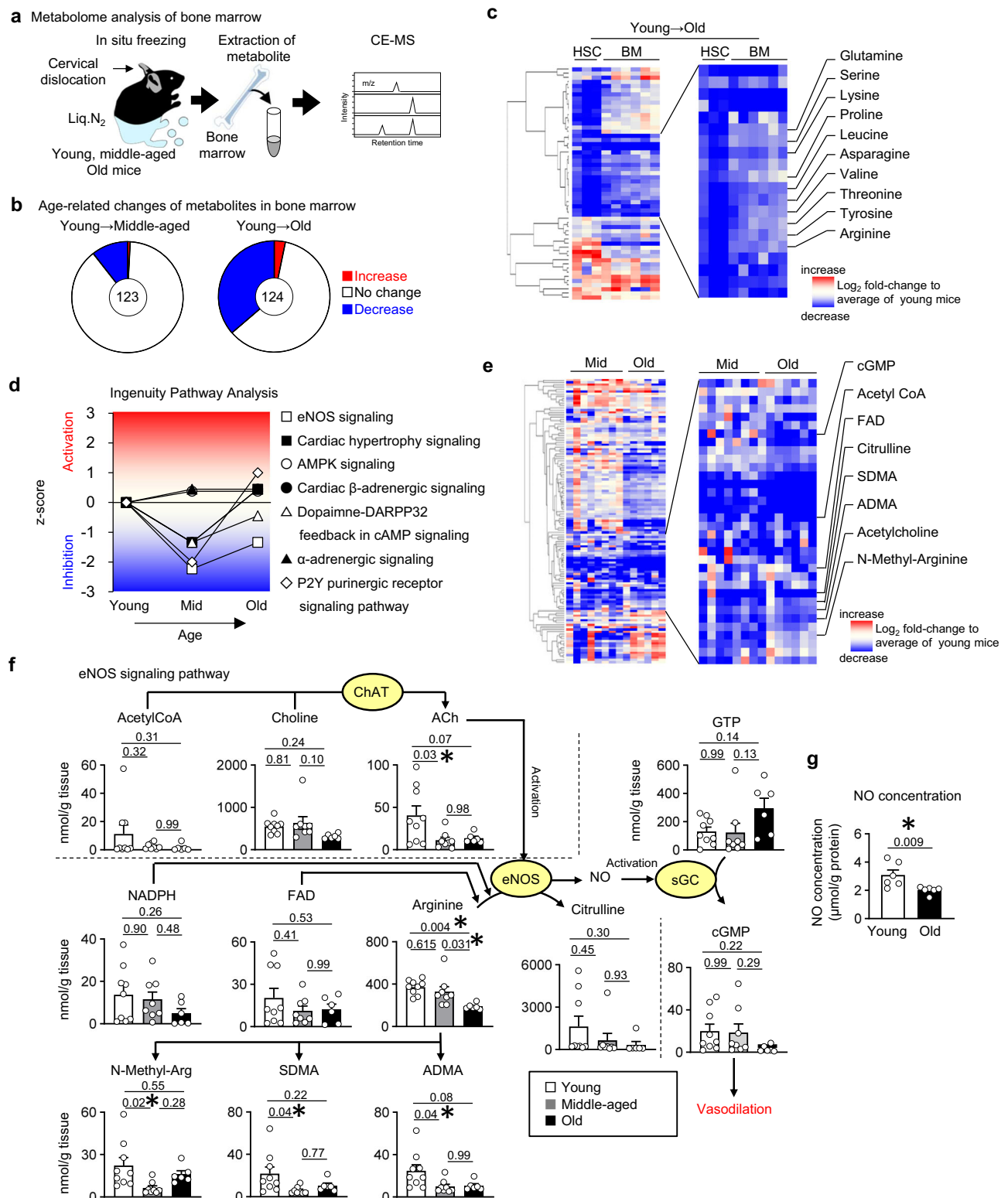
Fig. 3 | Old BM tissue has a metabolic profile indicative of decreased NO signaling. a Procedure for BM tissue metabolomics using an in situ freezing technique. **b** Classification of metabolites that increased, remained unchanged, or decreased in comparison to young to middle-aged BM (left) or young to old BM (right). The number of metabolites measured is displayed in the center of each chart. Values are mean ± SEM (**f**, **g**). **f** One-way ANOVA with Tukey–Kramer test. **g** Two-sided Mann–Whitney U test. **c** Cluster analysis of metabolites that increased or decreased during aging in HSC and BM. **d** Ingenuity pathway analysis based on changes in metabolite levels during aging using young mice as a reference. **e** Cluster analysis of metabolites that

increased or decreased in middle-aged or old BM tissues compared to young BM tissue. **f** Concentrations of NOS and NO signaling-related metabolites in BM tissues of young, middle-aged, and old mice. **a**–**f** young, $n = 9$; middle-aged, $n = 8$; old, $n = 6$ biological replicates. **g** NO concentrations in BM of young and old mice (young, $n = 6$; old, $n = 6$ biological replicates). Values are mean ± SEM (**f**, **g**). **f** One-way ANOVA with Tukey–Kramer test. **g** Two-sided Mann–Whitney U test. *$p < 0.05$. Source data are provided with this paper.
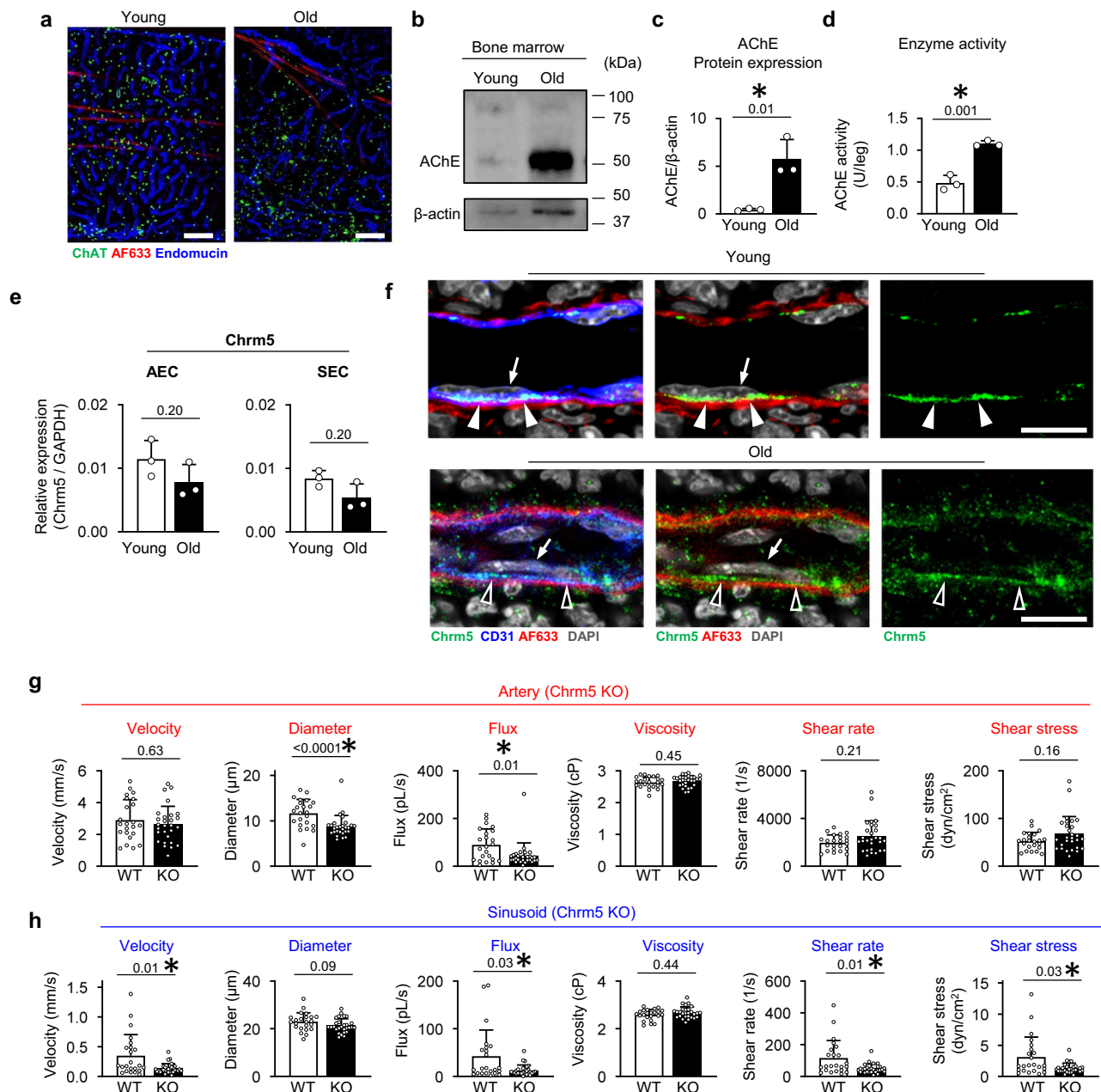
Fig. 4 | Non-neurogenic ACh, degradation of which is enhanced with age, maintains BM blood flow via Chrm5. a Immunohistochemical images of young and old ChAT^{BAC}-eGFP mice (ChAT$^+$ cell, green; AF633$^+$ artery, red; endomucin$^+$ sinusoid, blue). Bar = 100 μm. **b** Western blot analysis of AChE protein in BM lysates from young and old mice. **c** Protein levels of AChE in young and old BM evaluated by Western blotting (young, $n = 3$; old, $n = 3$ biological replicates). **d** AChE activity in young and old BM (young, $n = 3$; old, $n = 3$ biological replicates). **e** qPCR analysis of Chrm5 expression in AEC and SEC from young and old mice ($n = 3$ biological replicates). **f** Immunohistochemical analysis of Chrm5 expression on BM blood vessel of young and old mice (Chrm5, green; AF633$^+$ artery, red; CD31$^+$ endothelium, blue; DAPI, grey). Open and closed arrowheads indicate Chrm5 expression sites. Arrows indicate endothelial cells. Bar = 10 μm. **g, h** Hemodynamic parameters of arteries (**g**) and sinusoids (**h**) in BM of wild-type and Chrm5 KO mice (WT artery, $n = 23$; KO artery, $n = 28$; WT sinusoid, $n = 23$; KO sinusoid, $n = 28$ biological replicates). Values are mean ± SD (**c**–**h**). **c**, **d** Two-sided Student's t-test, **e**–**h** Two-sided Mann–Whitney U test. *$p < 0.05$. Source data are provided with this paper.

cells also tended to increase in old BM compared to young BM. These results suggest that increased AChE activity in hematopoietic cells contributes to the age-related decrease in BM ACh.

Loss of Chrm5 or pharmacological inhibition of muscarinic receptors phenocopies microcirculation of old BM

To understand the role of ACh in BM microcirculation, we screened for ACh receptors (AChRs) specifically expressed in mouse BM vessels. AChRs include nicotinic receptors, barrel-like channels formed by a combination of multiple subunits (α1–α10, β1–β4, δ, γ, and ε), and

muscarinic receptors (Chrm1-5), G protein receptors[48]. Quantitative PCR (qPCR) analysis demonstrated that among AChRs, cholinergic receptor nicotinic alpha 2 (Chrna 2), Chrna 5, and muscarinic AChR 5 (Chrm5) were expressed in both arterial EC (AEC) and sinusoidal EC (SEC), but other AChRs (Chrna1, 3, 4, 6–10, Chrnb1-4, Chrnd, Chrng, Chrne, and Chrm1-4) were not detected (Fig. 4e, Supplementary Fig. 6a, b). Immunohistochemical and flow cytometry analysis also confirmed protein expression of Chrm5 on mouse BM AECs and SECs (Fig. 4f, Supplementary Fig. 6c, d); Chrm5 expression was also detected in AECs from old BM (Fig. 4e, f). To determine whether the loss of

Chrm5 causes an aging-like condition in BM, we compared the BM metabolic profile of Chrm5 knockout (Chrm5 KO) mice and its ability to produce NO versus that of wild-type (WT) mice. Compared to WT, Chrm5KO mice had decreased levels of some amino acids in the BM and decreased arterial NO levels. (Supplementary Fig. 6e, f, Supplementary Table 5).

To study the role of Chrm5 in BM microcirculation, we compared hemodynamics in BM of Chrm5 KO mice with those of WT mice[49]. Compared to WT mice, Chrm5 KO mice had smaller arterial diameters and less blood flux in calvarial and tibial BM (Fig. 4g, Supplementary Fig. 7a, b). Meanwhile, blood velocity and flux in BM sinusoids of Chrm5 KO mice were reduced compared to those of WT mice (Fig. 4h, Supplementary Fig. 7a, b). In contrast, diameters and intravascular volumes of sinusoids were similar between WT and Chrm5 KO mice (Fig. 4h, Supplementary Fig. 7a–c). When we compared hematopoietic phenotypes of Chrm5 KO mice with those of WT mice, we did not observe any age-related changes, such as an increase in HSCs, in KO mice compared to WT controls. This suggests that a reduction in blood flow alone is not sufficient to accelerate emergence of age-related phenotypes in HSCs already present in the BM (Supplementary Fig. 7d).

Next, to rule out the possibility that muscarinic AChR function, either developmental or extra-BM, contributes to the phenocopied microcirculation of old BM, the muscarinic AChR antagonist, scopolamine, was locally administered to the calvarial BM of adult mice and BM blood flow was monitored by intravital imaging[38] (Supplementary Fig. 8a). After local scopolamine administration, BM arteries constricted and arterial blood flow was reduced (Supplementary Fig. 8b, c). In BM sinusoids, blood flow velocity and flux were reduced after scopolamine administration (Supplementary Fig. 8d). This scopolamine-induced reduction in arterial and sinusoidal blood flow was reversed by administration of the NO donor, sodium nitroprusside (SNP) (Supplementary Fig. 8b–d). These data suggest that suppression of muscarinic ACh signaling reproduces the impaired blood flow in old BM.

Suppression of NO signaling phenocopies microcirculation of old BM

To investigate the role of NO in maintaining BM blood flow, we screened for NOS isozymes expressed in mouse BM ECs. eNOS expression was detected in both AECs and SECs with AECs showing significantly higher eNOS expression than SECs (Fig. 5a). eNOS was also expressed in AECs and SECs from aged BM (Supplementary Fig. 9a). Immunohistochemical analysis confirmed expression of eNOS protein, particularly in AECs ensheathed by vascular smooth muscle cells (Fig. 5b, Supplementary Fig. 9b). To study the role of eNOS in BM microcirculation, we compared vascular network properties in BM of eNOS knockout (eNOS KO) mice with those of WT mice. Morphologically, there were no significant differences in BM vascular architecture between WT and eNOS KO mice in both arteries and sinusoids (Fig. 5c), and BM vessel density was comparable between the two groups (Fig. 5d). On the other hand, in vivo imaging analysis of calvarial and tibial BM showed smaller arterial diameters and reduced sinusoidal blood flow velocity in eNOS KO mice compared to WT mice, while the diameter and intravascular volume of sinusoids were similar between WT and eNOS KO mice (Fig. 5e, f, Supplementary Fig. 9c–e). To determine whether the loss of eNOS causes an aging-like condition in BM, we compared BM metabolic profiles of eNOS KO mice to those of WT mice. Compared to WT, eNOS KO mice had decreased levels of 11 amino acids and total amino acid concentration in the BM (Supplementary Fig. 10a, Supplementary Table 6).

To rule out extra-BM function of eNOS on BM blood flow, given the high blood pressure in eNOS KO mice (Supplementary Fig. 10b), the NOS inhibitor NG-Nitro-L-arginine methyl ester (L-NAME) was locally administered into calvarial BM of WT mice and BM blood flow

was monitored by intravital imaging (Fig. 5g). After local administration of L-NAME without changes in systemic blood pressure and heart rate[38], BM arteries constricted and arterial blood flow was reduced (Fig. 5h, j, Supplementary Movie 1). In BM sinusoids, blood flow velocity and flux were reduced after L-NAME administration (Fig. 5i, k, Supplementary Movie 1). This L-NAME-induced reduction in arterial and sinusoidal blood flow was reversed by administration of SNP (Fig. 5h–k). Control experiments with local administration of PBS without L-NAME showed no changes in BM blood flow in either arteries or sinusoids (Supplementary Fig. 10c, d). These results suggest that suppression of NO-induced vasodilation reproduces the impaired blood flow in old BM.
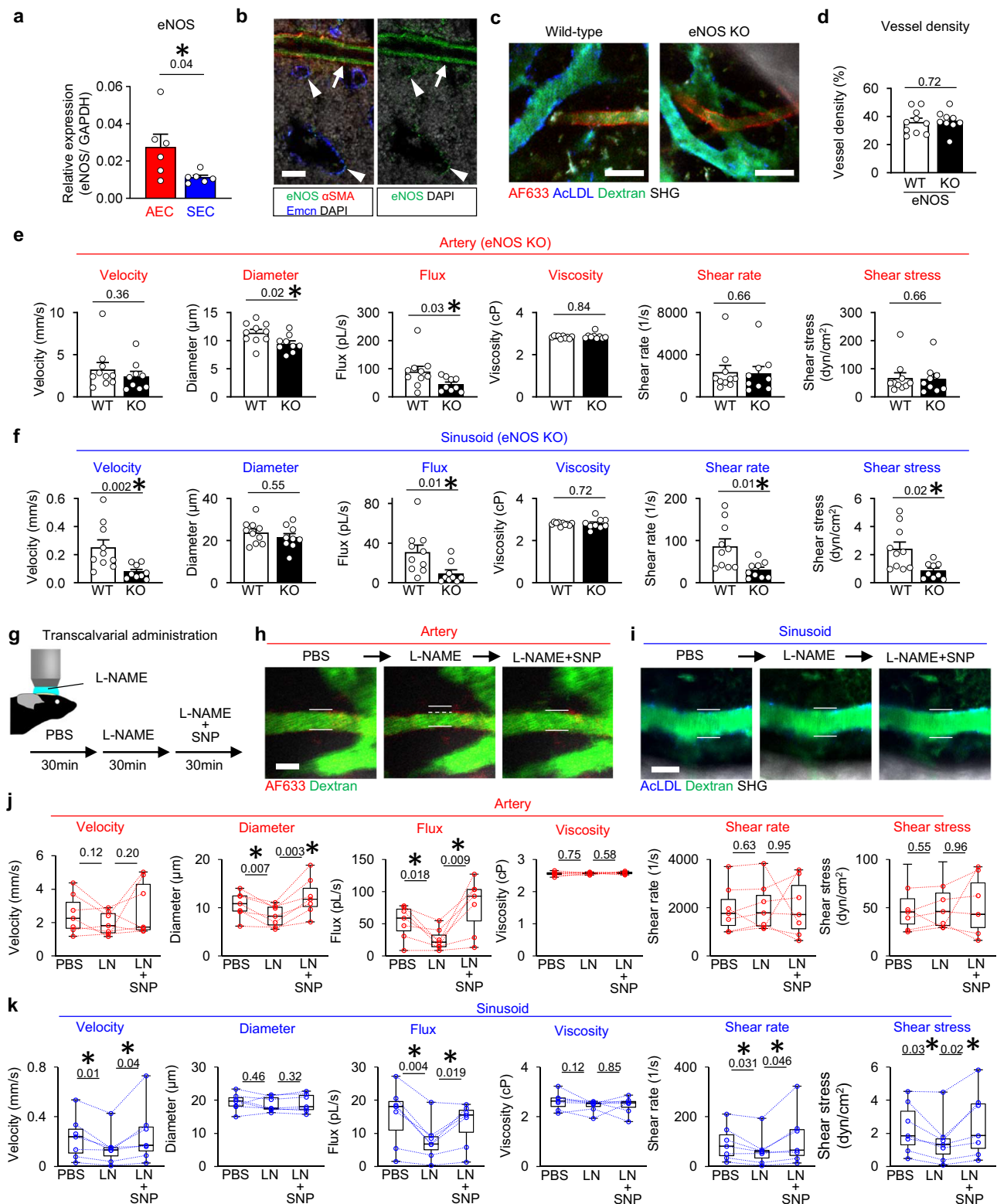
Piezo1 is a druggable target for TEM defects in old BM

Next, we examined whether NO maintains shear stress in BM sinusoids and promotes TEM of HSPCs. We injected HSPCs obtained from ubiquitin (Ubc)-GFP mice into recipients and analyzed TEM processes using multiphoton intravital microscopy with or without local L-NAME administration (Fig. 6a). To evaluate TEM efficiency, the time from HSPC adhesion in sinusoids to completion of extravascular migration was measured as Δt^{TEM} (Fig. 6b). Local administration of L-NAME prolonged Δt^{TEM} of HSPCs, while additional SNP administration shortened it (Fig. 6c). Furthermore, eNOS KO recipients injected with Ubc-GFP$^+$ HSPCs had prolonged Δt^{TEM} compared to WT recipients (Fig. 6d). The prolonged Δt^{TEM} in eNOS KO recipients was shortened to the same level as in WT recipients after local SNP administration (Fig. 6d).

We further investigated how HSPC TEM is promoted by arterial blood flow and the resulting shear stress in sinusoids. Vessel wall shear stress activates the mechanoreceptor, Piezo1, which then initiates calcium signaling and promotes leucocyte trafficking during inflammation[33]. Based on this report, we examined the involvement of Piezo1 on BM ECs in HSPC TEM (Supplementary Fig. 11a). Additional administration of a Piezo1 inhibitor GdCl₃ abolished the Δt^{TEM}-shortening effect of SNP in eNOS KO mice (Fig. 6d). To test whether GdCl₃ affected blood flow, we measured blood flow in the BM before and after local administration of GdCl₃. The results showed no change in arterial blood flow, but there was a decrease in flow velocity and shear stress, possibly due to sinusoidal dilation (Supplementary Fig. 11b). These results suggest that GdCl₃ treatment reduces Piezo1 activity in sinusoids through both direct pharmacological inhibition and a decrease in shear stress.

Furthermore, local administration of a Piezo1 agonist, Yoda1, shortened Δt^{TEM} of transplanted Ubc-GFP$^+$ HSPCs of eNOS KO mice, whereas no effect of Yoda1 on blood flow was observed under these conditions (Fig. 6e, Supplementary Fig. 11c). These results suggest that NO synthesized by eNOS maintains shear stress-induced activation of Piezo1 on ECs to maintain a BM environment favorable for HSPC TEM.

We had already determined that NO levels and sinusoidal shear stress of old BM were lower than those of young BM (Figs. 2e, 3g). To investigate whether the age-related decrease in NO and sinusoidal shear stress affects TEM of HSPCs, we injected Ubc-GFP$^+$ HSPCs into young and old mice and compared Δt^{TEM} in the presence or absence of NO and/or Piezo1 modulators. Δt^{TEM} of HSPCs in old BM was longer than that in young BM (Fig. 6f). The prolonged Δt^{TEM} of HSPCs in old BM was shortened by local SNP administration. Next, we evaluated the contribution of shear stress to the NO-dependent prolongation of Δt^{TEM} in old BM. Piezo1 was expressed in SECs of old BM (Fig. 6g). The Δt^{TEM}-shortening effect of SNP was abolished by local GdCl₃ administration into BM of old mice (Fig. 6f). Activation of Piezo1 by local Yoda1 administration shortened Δt^{TEM} of HSPCs into old BM (Fig. 6h). At this time, we observed no effect on blood flow in aged mice (Supplementary Fig. 11d). We further analyzed the correlation between Δt^{TEM} and sinusoidal shear stress at the site where TEM occurred (Fig. 6c, d and f) (excluding GdCl₃-treated mice). We found a negative correlation between Δt^{TEM} of HSPCs and sinusoidal shear stress (Fig. 6i). These

a eNOS

b eNOS αSMA Emcn DAPI / eNOS DAPI

c Wild-type / eNOS KO — AF633 AcLDL Dextran SHG

d Vessel density

e Artery (eNOS KO) — Velocity, Diameter, Flux, Viscosity, Shear rate, Shear stress

f Sinusoid (eNOS KO) — Velocity, Diameter, Flux, Viscosity, Shear rate, Shear stress

g Transcalvarial administration — L-NAME; PBS 30min → L-NAME 30min → L-NAME + SNP 30min

h Artery — PBS → L-NAME → L-NAME+SNP — AF633 Dextran

i Sinusoid — PBS → L-NAME → L-NAME+SNP — AcLDL Dextran SHG

j Artery — Velocity, Diameter, Flux, Viscosity, Shear rate, Shear stress

k Sinusoid — Velocity, Diameter, Flux, Viscosity, Shear rate, Shear stress

results suggest that old BM is less suitable for TEM than young BM due to reduced NO production, resulting in decreased shear stress in the sinusoids, which can be pharmacologically targeted by a Piezo1 agonist.

Arterial ACh-NO signal and subsequent sinusoidal shear stress are therapeutic targets for improved homing

Based on these findings, we investigated whether arterial ACh-eNOS signaling and sinusoidal Piezo1 activation by shear stress regulate

homing of transplanted HSPCs. We confirmed the reduction in NO levels in the BM arteries of hematopoietic cell-specific ChAT knockout (ChAT-cKO) mice (Supplementary Fig. 12a). Next, we compared homing efficiency of transplanted HSPCs to BM using ChAT-cKO or WT mice as recipients (Fig. 7a). BM homing efficiencies of transplanted HSCs, MPP1s, and LSK cells were lower in ChAT cKO recipients compared to WT recipients (Fig. 7b, Supplementary Fig. 12b). As we tested whether loss of the ACh receptor also affects homing, we found that Chrm5 KO mice also had reduced homing efficiency of HSCs and some

Fig. 5 | Suppression of NO signaling phenocopies microcirculation of old BM.
a qPCR analysis of eNOS expression in AEC (*n* = 6 biological replicates) and SEC
(*n* = 6 biological replicates). **b** Immunohistochemical analysis of eNOS expression in
BM blood vessels. Arrows, αSMA⁺ artery (red), arrowheads, sinusoids (blue), eNOS
(green), DAPI (grey). Bar = 10 μm. **c** Intravital imaging of wild-type or eNOS KO
calvarial BM. AF633⁺ artery, red, AcLDL⁺ sinusoid, blue, blood flow (dextran), green,
bone (SHG second harmonic generation), grey. Bar = 20 μm. **d** BM blood vessel
density of wild-type and eNOS KO mice (WT, *n* = 10; KO, *n* = 9 biological replicates).
e, **f** Hemodynamic parameters of arteries (**e**) and sinusoids (**f**) in BM of wild-type
and eNOS KO mice (WT artery, *n* = 10; KO artery, *n* = 9; WT sinusoid, *n* = 10; KO
sinusoid, *n* = 9 biological replicates). **g** Procedure for intravital imaging of BM with
transcalvarial administration of L-NAME (1 mM) and sodium nitroprusside (SNP,

100 μM). **h** Representative timelapse images of arterial vasoconstriction induced by
L-NAME. AF633⁺ artery, red, blood flow (dextran), green. Bar = 10 μm.
i Representative intravital imaging of a sinusoid after administration of L-NAME and
SNP. AcLDL⁺ sinusoid, blue, blood flow (dextran), green, bone (SHG, second har-
monic generation), grey. Bar = 20 μm. **j**, **k** Hemodynamics of arteries (**j**) and sinu-
soids (**k**) after transcalvarial administration of L-NAME in BM (artery, *n* = 7; sinusoid,
n = 7 biological replicates). Values are mean ± SEM (**a**–**f**). **a**–**f** Two-sided
Mann−Whitney *U* test. **j**, **k** Each box represents the first through third quartiles, the
horizontal line represents the median, and the whiskers extend from the lower and
upper bounds of the box to the maximum or minimum value. Paired two-sided
Student's *t*-test. *$p < 0.05$. Source data are provided with this paper.

mature blood cells to the BM (Supplementary Fig. 12c). Next, we
compared homing efficiency of transplanted HSPCs to BM using eNOS
KO or WT mice as recipients. BM homing efficiency of transplanted
HSCs and other fractions in eNOS KO recipients was lower than in WT
recipients (Fig. 7c, Supplementary Fig. 12d, e). Administration of SNP
to eNOS KO recipients increased homing efficiency of HSCs and LSK
cells without any population change of BM and peripheral blood cells
(Fig. 7c, Supplementary Figs. 12d, 13a, b). To test whether shear stress is
involved in HSPC homing to BM, we evaluated homing efficiency of
transplanted HSPCs upon inhibition or activation of Piezo1. Homing
efficiency of HSCs was lower in GdCl₃-treated BM than in controls (Fig.
7d, Supplementary Fig. 14a). On the other hand, administration of
Yoda1 increased homing efficiency of HSCs (Fig. 7e). These results
indicate that arterial ACh-NO signaling and subsequent sinusoidal
shear stress are responsible for HSPC homing and that there is room
for improvement of HSPC homing with Piezo1 activation.

**Reduced homing efficiency due to decreased NO and inactiva-
tion of Piezo1 in old BM can be treated pharmacologically**
We compared changes in BM homing efficiency of transplanted HSPCs
in young and old recipients without irradiation (Fig. 7f). Consistent
with a previous report[8], BM homing efficiency of transplanted HSPCs,
including HSCs, MPP1s, and LSK cells, was lower in old recipients than
in young recipients (Fig. 7g, Supplementary Fig. 14b). Administration
of SNP to old recipients improved homing efficiency of HSCs (Fig. 7g).
Furthermore, administration of Yoda1 improved BM homing efficiency
of transplanted HSCs in old recipients compared to DMSO-treated old
recipients without conditioning (Fig. 7h). We further examined homing
efficiency and hematopoietic recovery after transplantation in a more
clinically relevant setting with preconditioning. We examined whether
homing efficiency of transplanted HSPCs in irradiated old recipients is
improved by enhanced NO signaling (Fig. 7i). Homing efficiency of
transplanted HSCs, MPP1s, and BM mononuclear cells (BMMNCs) in
irradiated old recipients was reduced, as previously reported[8] (Fig. 7j,
Supplementary Fig. 14c). In these irradiated old recipients, impaired
homing efficiency of transplanted HSCs was improved by administra-
tion of SNP (Fig. 7j). Finally, we investigated whether hematopoietic
recovery could be enhanced by pharmacological activation of Piezo1
using Yoda1 after HSPC transplantation into irradiated old mice (Fig.
7k). In this model, the 1 month survival rate was 50% in young reci-
pients and 0% in old recipients (Fig. 7l). Improved hematopoietic
recovery and donor-derived HSC chimerism in BM were observed in
old recipients treated with Yoda1. (Supplementary Fig. 15a, b), and the
survival rate of Yoda1-treated old mice was improved (Fig. 7l).

As shown in the HSCT[50] and parabiosis[51] models, long-term
engraftment capacity declines in aged recipients. We tested whether
Yoda1 administration ameliorates the age-related decline in engraft-
ment (Supplementary Fig. 15c). Chimerism analysis up to 12 weeks
after HSCT showed higher donor chimerism in peripheral blood in the
Yoda1 group compared to the control group (Supplementary Fig. 15d).
These findings suggest that supplementation of NO or activation of
Piezo1 can ameliorate engraftment failure in aged recipients.

Discussion
The mechanism of HSPC engraftment in BM and its improvement is a
clinically important topic, but so far only attempts to increase the
number of transplantable HSPCs ex vivo[52–54] or to improve the homing
ability of HSPCs have been made[18,55]. In this study, we found that non-
neurogenic ACh induces endothelial NO production in BM, dilates
arteries, and increases perfusion of BM. As a consequence, we found
that increased blood flow upregulates sinusoidal shear stress and
promotes TEM of HSPCs through activation of the mechanoreceptor,
Piezo1, which facilitates TEM, an essential step for BM homing and
engraftment. Knockout of genes associated with this cascade or local
inhibition both reduced HSPC and mature blood cell homing to BM.
These findings offer the possibility of improving HSPC homing in a
different way than those attempted previously. It has been reported
that shear stress activates Piezo1 and subsequent downstream calcium
signaling in endothelial cells, facilitating TEM of lymphocytes by
actomyosin contraction and weakening of endothelial cell adhesion[33].
Under intravital microscopic imaging, as several HSPCs that could not
migrate smoothly through the endothelium were released back into
circulation, Δtᵀᴱᴹ was used as an indicator of the suitability of sinusoids
for TEM in this study. Although we focused on the migration process,
attachment of HSPCs to sinusoidal endothelial cells is also critical for
homing, and higher shear stress prevents attachment of HSPCs to
sinusoidal vessel walls[15]. These observations collectively indicate that
controlling shear stress to keep it within the appropriate range is
important for homing of HSPCs in BM. This mechanism contributes
not only to generating appropriate wall shear stress in sinusoids, but
also to efficient use of oxygen and metabolic resources supplied
through limited vessels in cortical bone[56]. In this study, we identified a
decrease in levels of metabolites such as amino acids with age, and we
found that the underlying decrease in BM blood flow reduces the
homing efficiency of HSPCs. On the other hand, the decrease in
metabolites such as amino acids with age may be due not only to a
decrease in blood flow, but also to changes in the proportion of BM cell
fractions and changes in metabolic characteristics such as intracellular
protein degradation and energy generation that occur with age (Fig.
1h)[57–59]. In this study, we confirmed that there were no age-related
changes in the proportion of BM myeloid cells or levels of metabolites
(Supplementary Fig. 4b, 4c, 4d, 4e). In contrast, changes in the number
of myeloid cells with aging remain controversial[42,60–64], and there are
reports that they vary with infection[65] and the environment in which
they are kept[60]. Thus, we could not completely rule out the possibility
that other cells were also involved, so this is a topic for future research.

Decreased graft engraftment in HSCT to elderly recipients is a
clinical issue that remains incompletely understood[8,66]. We also found
that this set of homing mechanisms is attenuated in aged mice as ACh
decreases. Mechanistically, both the amount and activity of AChE
within hematopoietic cells are increased in aged BM (Fig. 4c, d). We
have found that administration of AChE inhibitors to recipients at
various doses and routes does not improve HSPC homing to recipient
BM (data not shown). Because BM arteries decrease with age[67], simply
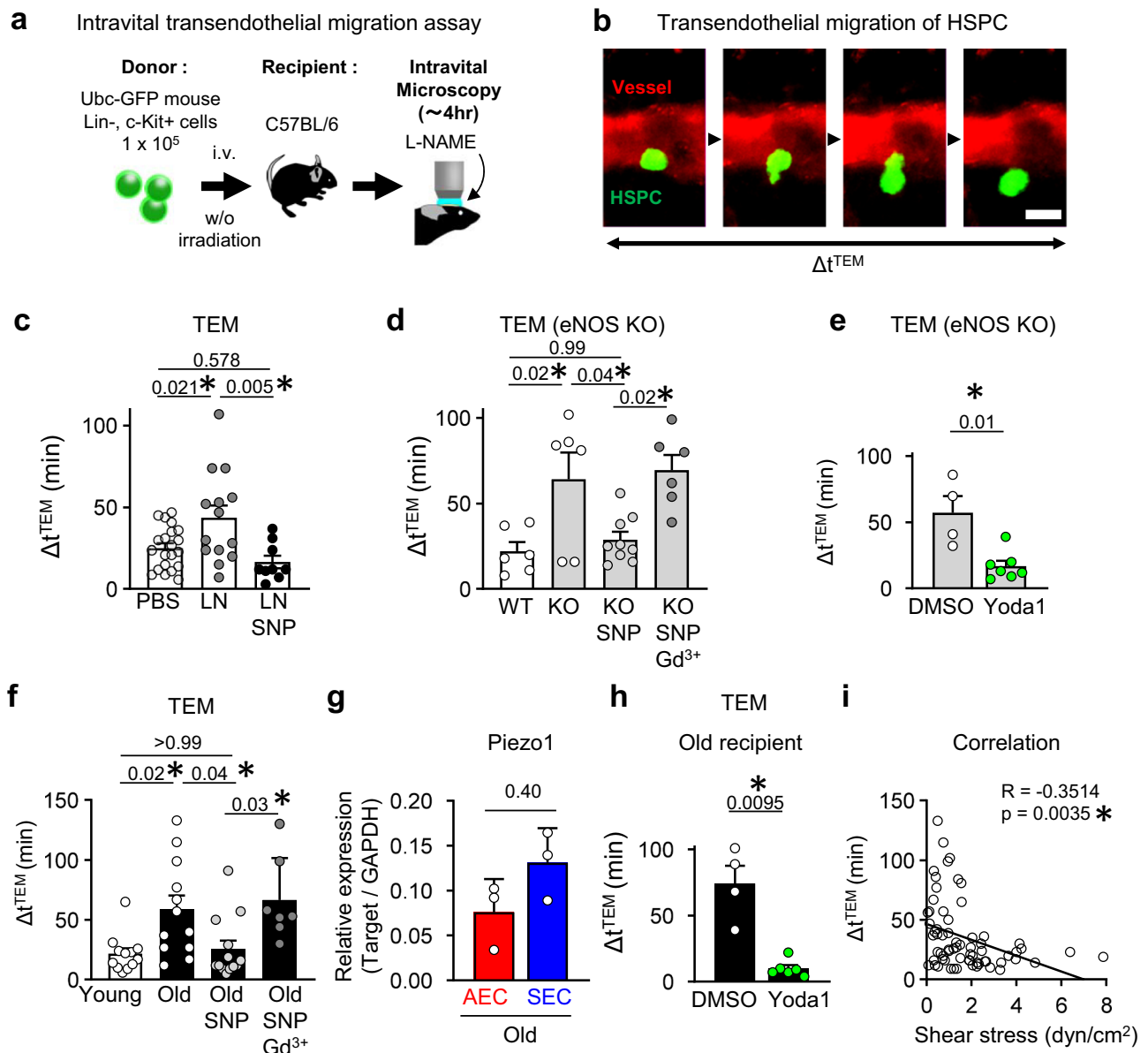intervening with BM blood flow may not be sufficient to improve HSPC

Fig. 6 | Piezo1 can be targeted pharmacologically for TEM defects in old recipients. a Procedure of in vivo assay. **b** Transendothelial migration of HSPCs observed by intravital microscopy. Bar = 10 μm. **c** The time required for transendothelial migration of HSPCs in BM after L-NAME (LN) and SNP administration (PBS, 21 cells / 8 mice; LN, 14 cells / 7 mice; LN + SNP, 9 cells / 2 mice). **d** Time required for TEM of HSPCs into BM of wild-type (WT), or eNOS KO mice treated with vehicle, SNP, or SNP+Gd^{3+} (WT, 6 cells / 3 mice; KO, 6 cells / 3 mice; KO + SNP, 9 cells / 3 mice; KO + SNP+Gd^{3+}, 6 cells / 2 mice). **e** Time required for TEM of HSPCs into BM of eNOS KO mice after DMSO or Yoda1 administration (DMSO, 4 cells / 3 mice; Yoda1, 7 cells / 3 mice). **f** Time required for TEM of HSPCs in BM of young and old mice treated with vehicle, SNP, or SNP+Gd^{3+} (young, 12 cells / 6 mice; old, 12 cells / 5 mice; old+SNP, 13 cells / 6 mice; old+SNP+Gd^{3+}, 7 cells / 6 mice). **g** qPCR analysis of Piezo1 expression in AEC and SEC from old mice ($n = 3$ each). **h** Time required for TEM of HSPCs into BM of old mice after DMSO or Yoda1 administration (DMSO, 4 cells / 2 mice; Yoda1, 6 cells / 2 mice). **i** Correlation between shear stress and time required for TEM of HSPC (67 cells / 25 mice). Values are mean ± SD (**g**) and mean ± SEM (**c** –**h**) **c**–**f** One-way ANOVA with Tukey–Kramer test. **e**–**h** Two-sided Mann–Whitney U test. **i** Pearson's correlation coefficient (r) and p-values (Two-sided) are shown. *$p < 0.05$. Source data are provided with this paper.

homing in aged recipients. On the other hand, pharmacological activation of Piezo1, which is stably expressed in sinusoidal vessels that maintain their structure even in aging BM, improved homing and engraftment in aged BM. Understanding increased AChE expression in aging B cells and other blood cells and its epigenetic basis may allow for more efficient improvement of HSPC homing to aging BM. Notably, according to the Tabula Muris Senis scRNA-seq database, premature B cells expressing the AChE gene already begin to appear in BM of middle-aged mice, with a corresponding decrease in ACh concentration (Fig. 3f). On the other hand, concentrations of choline and arginine, substrates of ChAT and eNOS respectively, were not changed in middle-aged BM compared with those in young mice (Fig. 3f). These data suggest that reduction of ACh-induced blood flow commencing in middle-aged BM reduces supplies of choline and arginine to old BM, and further reduces blood flow. Production of ACh by T cells in addition to B cells in aging BM may be an adaptive response to maintain local blood flow by accelerating ACh production while antagonizing its degradation by AChE (Fig. 4c, d). Although SNP administration experiments in this study did not show any population change in BM cells, NO acts directly on HSPCs in BM to regulate their dynamics[68,69], and it remains to be determined whether NO, which is reduced in aging BM, affects HSPCs in the niche (Supplementary Fig. 13a, b).
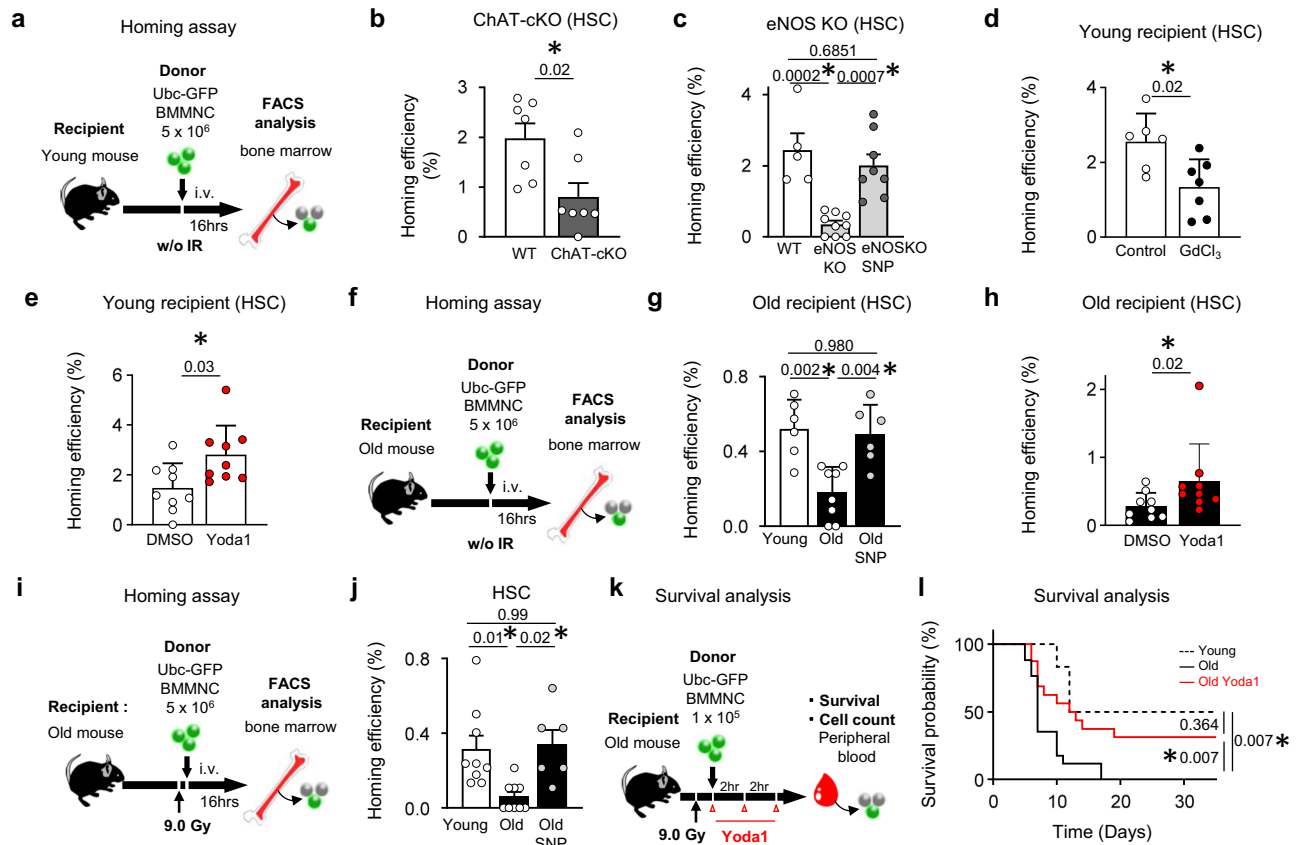
Fig. 7 | Arterial ACh-NO signaling and subsequent sinusoidal shear stress reduction can be pharmacologically targeted for HSPC homing and survival in old recipients. a Design of unconditioned homing assay using young mice as recipients. **b** Homing efficiency of HSCs in BM of wild-type (WT) or ChAT cKO mice (WT, $n = 7$; cKO, $n = 7$ biological replicates). **c** Homing efficiency of HSCs in BM of WT or eNOS KO mice with or without SNP treatment (WT, $n = 5$; KO, $n = 9$; KO + SNP, $n = 8$ biological replicates). **d** Homing efficiency of HSCs into BM of young recipients after PBS or GdCl$_3$ administration (PBS, $n = 6$, GdCl$_3$, $n = 7$ biological replicates). **e** Homing efficiency of HSCs in young mice after DMSO or Yoda1 administration (DMSO, $n = 9$; Yoda1, $n = 9$ biological replicates). **f** Design of homing assay using old mice as recipients. **g** Homing efficiency of HSCs in BM of young or

old mice with or without SNP treatment (young, $n = 6$; old, $n = 8$; old+SNP, $n = 6$ biological replicates). **h** Homing efficiency of HSCs in old mice after DMSO or Yoda1 administration (DMSO, $n = 9$; Yoda1, $n = 9$ biological replicates). **i** Design of homing assay using irradiated old mice as recipients. **j** Homing efficiency of HSCs in BM of irradiated young, old, SNP-treated old mice (young, $n = 9$; old, $n = 9$; old+SNP, $n = 6$ biological replicates). **k** Design of survival analysis of old recipients after myeloablative BM transplantation. **l** Survival of young, old, Yoda1-treated old mice after BM transplantation (young, $n = 6$; old, $n = 17$; old+Yoda1, $n = 16$ biological replicates). Values are mean ± SEM (**b–j**). **b–h** Two-sided Mann–Whitney U test. **c–j** One-way ANOVA with Tukey–Kramer test. **l** log-rank (Mantel–Cox) test. *$p < 0.05$ Source data are provided with this paper.

In this report, we focused on the homing-promoting effect of eNOS expressed in the BM vasculature. Recently, the HSC subfraction, which autonomously produces NO through eNOS, has been shown to play an important role in the hematopoietic hierarchy and immune regulation[70]. Furthermore, other NOS isozymes, such as nNOS and iNOS, are also expressed in the BM. Since functions of osteoclasts and osteoblasts involved in HSPC mobilization are maintained by NOS, it is possible that they are also involved in homing, which is a similar phenomenon in terms of altering spatiotemporal dynamics of HSPCs[71–73]. In addition, NOS inhibitor-treated HSPCs were highly proliferative and eNOS, which is expressed by HSPC themselves, regulates membrane localization of Cxcr4 to control mobilization and homing[74,75]. Due to the short half-life of NO (<1 s), NO produced by multiple cell types is likely to prove important in various events in the local BM[76]. Therefore, to further investigate NO's role in BM hematopoiesis, intravital imaging techniques are instrumental in capturing phenomena, including NO production in vivo, in real-time at the specific BM site. However, it is difficult to simultaneously measure blood flow in a large volume of BM with the local blood flow measurement method used in this study, and verification of the blood flow dynamics in the arterial system and sinusoidal vessels of the entire BM after a specific time of stimulation with each drug is a future issue.

Neurotransmitters derived from BM nerves reportedly regulate HSPC mobilization from BM and hematopoietic recovery after stress[77–81]. ACh secreted by sympathetic cholinergic fibers that originate in the BM after BMT also activates mesenchymal stem cells (MSCs) via α7 nicotinic ACh receptors (α7nAChR) to produce Cxcl12, promoting HSC quiescence[82]. Recently, it has been shown that ACh derived from BM blood cells, especially B cells, is important for steady-state hematopoiesis, acting through α7nAChR on mesenchymal niche cells[46]. In the present study, we found that BM blood flow is regulated via the ACh-NO cascade and involved in HSPC homing via another ACh receptor, Chrm5[83]. ACh is an evolutionarily conserved signaling molecule that is produced not only by neurons and non-neuronal cells in vertebrates and invertebrates, but also by organisms without neuronal systems, such as bacteria and plants[84–87]. Thus, ACh may have evolved the ability to use multiple receptors in the BM to reliably maintain hematopoiesis.

In summary, we show that the age-related decline in the non-neurogenic ACh-Chrm5-NO-shear stress-Piezo1 cascade is responsible for defective homing and engraftment in old recipients (Supplementary Fig. 15e). Pharmaceutical interventions may further improve HSC-based medicine.

Methods

Mice

C57BL/6 mice were purchased from Japan SLC or CLEA Japan. Evi1-IRES-GFP knockin (Evi1-GFP) mice[36] were provided by Dr. Mineo Kurokawa at the University of Tokyo. eNOS-deficient mice[88] were provided by the Tsutsui laboratory at the University of the Rykyus. ChAT[BAC]-eGFP mice (Strain #:007902), Tie2-Cre mice (Strain #:008863), Ubc-GFP reporter mice (Strain #:004353), and mutant mice with targeted alleles for ChAT (ChAT[flox], Strain #:016920) were provided from the Jackson Laboratory. Chrm5 KO mice (B6;129-Chrm5[tm1], Strain #:541)[49] were provided from Center for Animal Resources and Development, Kumamoto University, respectively. ChAT[flox] mice were crossed with Tie2-Cre mice to obtain ChAT cKO mice. Mice were housed under a 12 h light–12 h dark cycle (8 a.m. to 8 p.m.) and fed ad libitum a standard CE-2 diet (CLEA Japan). All mice, except immature (6 week-old), middle-aged (12–14 month-old) and old (18–24 month-old) mice, were used in the experiment at 10–12 weeks of age. All experimental procedures were approved by the institutional review board of the National Institute of Global Health and Medicine and were performed according to guidelines (Protocol No. 2024-A006). Due to the limited number of aged and KO mice, we used both male and female mice in this study.

Reagents

AlexaFluor 488 AcLDL (Cat # L23380), AlexaFluor 633 (Cat # A30634) and Qdot 655 (Cat # Q21021MP) were purchased from Thermo Fisher Scientific. TRITC-Dextran 500 (Cat # 54194), Scopolamine hydrobromide (Cat # S0929), Gadolinium (III) chloride hexahydrate (Cat # G7532) and Sodium nitroprusside dehydrate (Cat # 71778) were obtained from Sigma-Aldrich. Yoda1 (Cat # 21904) were obtained from Cayman Chemical.

Antibodies

The following antibodies were used in this study: Anti-mouse CD4 (BD Biosciences, Cat # 550954, clone: RM4-5, Dilution ratio 1:100), Anti-mouse CD8a (BioLegend, Cat # 100734, clone: 53-6.7, Dilution ratio 1:100), Anti-mouse B220 (BD Biosciences, Cat # 552771, clone: RA3-6B2, Dilution ratio 1:100), Anti-mouse Ter-119 (BioLegend, Cat # 116228, clone: TER-119, Dilution ratio 1:100), Anti-mouse Gr1 (BioLegend, Cat # 108428, clone: RB6-8C5, Dilution ratio 1:100), Anti-mouse Mac1 (BD Biosciences, Cat # 550993, clone: M1/70, Dilution ratio 1:100), Anti-mouse Sca-1 (BioLegend, Cat # 122514, clone: E13-161.7, Dilution ratio 1:100), Anti-mouse c-Kit (BioLegend, Cat # 105826, clone: 2B8, Dilution ratio 1:100), Anti-mouse CD150 (BioLegend, Cat # 115904, clone: TC15-12F12.2, Dilution ratio 1:100), Anti-mouse CD48 (BioLegend, Cat # 103426, clone: HM48-1, Dilution ratio 1:100), Anti-Flt3 (BioLegend, Cat # 135310, clone: A2F10, Dilution ratio 1:100), Anti-CD34 (BD Biosciences, Cat # 560233, clone: RAM34, Dilution ratio 1:100), Anti-mouse IL7RA (BD Biosciences, Cat # 552543, clone: SB/199, Dilution ratio 1:100), Anti-CD45 (BioLegend, Cat # 103132, clone: 30-F11, Dilution ratio 1:100), Anti-CD31 (BD Biosciences, Cat # 551262, clone: MEC 13.3, Dilution ratio 1:100), Anti-VE-cadherin (eBioscience, Cat # 12-1441-82, clone: eBioBV13, Dilution ratio 1:100), Anti-Podoplanin (BioLegend, Cat # 127412, clone: 8.1.1, Dilution ratio 1:100), Anti-CD16/32 (BD biosciences, Cat # 553142, clone: 2.4-G2, Dilution ratio 1:100), Anti-Endomucin (Santa Cruz Biotechnology, Cat # sc-65495, clone: v.7c7, Dilution ratio 1:100), Anti-Chrm5 (My Bio Source, Cat # MBS9126416, Dilution ratio 1:100. Alomone Labs, Cat # AMR-006, Dilution ratio 1:100), Anti-α-SMA (Sigma, A2547, clone: 1A4; Dilution ratio 1:500), Anti-eNOS (Cell signaling, Cat # 32027, clone: D9A5L, Dilution ratio 1:100), Anti-AChE (Santa Cruz Biotechnology, sc-373901, clone: A-11, Dilution ratio 1:1000), Anti-β-actin (Sigma, Cat # A5316, clone: Ac-74, Dilution ratio 1:10000),

Flow cytometry

For hematopoietic cell analysis and sorting, BMMNCs were isolated by centrifugation and hemolysis of total BM (femur and tibia). BMMNCs were stained with antibodies for surface markers, including lineage, stem, and progenitor markers for 30 min[89,90]. Endothelial cells (ECs) were isolated by digestion of BM of mice injected intravenously with fluorophore-labelled antibody against Podoplanin 10 min before sacrifice[91]. Mouse femoral and tibial BM was flushed in 1 mL digestion solution (7 mg/mL Collagenase type I (Gibco), 1 mg/mL DNase I (Sigma) in PBS/2% FCS) and incubated at 37°C for 20 min. Digested BM was suspended by gentle pipetting, followed by filtration through 70 μm nylon mesh. Cells were washed by centrifugation in PBS/2% FCS and stained with antibodies against surface markers including TER-119, CD45, CD31, VE-cadherin and Sca-1 at 4°C for 30 min. Stained cells were analyzed by SORP FACSAriaIII (BD Biosciences). Data were analyzed using FlowJo™ software (version 10.7.1, Tree Star Inc).

CE-MS and ion chromatography (IC)-MS analysis

Sorted BM cells were washed with 5% mannitol and dissolved in ice-cold methanol (500 μL) containing internal standards (300 μM each of L-methionine sulfone and morpholinoethane sulfonic acid). Frozen femurs were plunged into ice-cold methanol (500 μL) containing internal standards (300 μM each of L-methionine sulfone and morpholinoethane sulfonic acid) and immediately flushed. Then 250 μL of ultrapure water (LC/MS grade; Wako) were added to these methanol solutions containing cells or BM lysate. 750 μL of the solution were transferred, and 500 μL of chloroform were added, followed by thorough mixing. The resulting suspension was centrifuged at 15,000 × g for 15 min at 4 °C. The upper aqueous layer was extracted with chloroform and then centrifugally filtered through a 5 kDa cutoff filter (Human Metabolome Technologies).

Quantification of metabolites in whole BM by CE-MS analysis was performed as described previously with slight modifications[37]. For analysis of HSPC, young, middle-aged and old BM samples, filtrates were concentrated with a vacuum concentrator (SpeedVac; Thermo) and dissolved in 100 μL of ultrapure water containing reference compounds (200 μM each of 3-aminopyrrolidine and trimesate) before CE-MS analysis. All CE-MS experiments were performed using an Agilent 1200 series mass spectrometer (Agilent). Data acquisition and data evaluation were performed using Agilent G2201AA ChemStation software[92]. Biological pathways that are upregulated and downregulated during aging were identified with Ingenuity Pathway Analysis (Qiagen). Principal component analysis was performed using R-Studio 1.3.1056 software.

For analysis of myeloid cells, and KO mice BM, filtered samples were analyzed by IC-MS. For metabolomic analysis of glycolytic metabolites and nucleotides, anionic metabolites were measured using an orbitrap-type MS (Q-Exactive focus; Thermo Fisher Scientific) connected to a high-performance IC system (ICS-5000 +, Thermo Fisher Scientific), which enabled highly selective and sensitive metabolite quantification due to IC-separation and the Fourier Transfer MS principle. The IC was equipped with an anion electrolytic suppressor (Thermo Scientific Dionex AERS 500) to convert the potassium hydroxide gradient into pure water before the sample entered the mass spectrometer. Separation was performed using a Thermo Scientific Dionex IonPac AS11-HC, 4 μm particle size column. The IC flow rate was 0.25 mL/min supplemented post-column with a 0.18 mL/min flow of MeOH. Potassium hydroxide gradient conditions for IC separation were as follows: from 1 mM–100 mM (0–40 min), 100 mM (40–50 min), and 1 mM (50.1–60 min) at a column temperature of 30 °C. The Q Exactive focus mass spectrometer was operated in ESI negative mode for all assays. A full mass scan (m/z 70 − 900) was performed at a resolution of 70,000. The automatic gain control target was set at 3×10^6 ions, and the maximum ion injection time was 100 msec. Source ionization parameters were optimized with the spray

voltage at 3 kV. Other parameters were: transfer temperature = 320 °C, S-Lens level = 50, heater temperature = 300 °C, Sheath gas = 36, and Aux gas = 10

Total products of the TCA cycle are the sum of levels of acetyl CoA, citrate, cis-aconitate, isocitrate, succinate, fumarate and malate. Total amino acids are the sum of levels of glycine, alanine, serine, threonine, valine, isoleucine, leucine, lysine, arginine, histidine, tyrosine, phenylalanine, tryptophan, methionine, cysteine, proline, glutamine, glutamate, asparagine and aspartate.

Determination of NO in BM

The NO concentration in murine BM was measured by QuantiChrom™ Nitric Oxide Assay Kit (BioAssay Systems). Mouse femoral and tibial BM were flushed and homogenized in 0.5 mL ice-cold PBS. Homogenate was centrifuged at $10000 \times g$ and supernatant was used to measure NO concentration according to the manufacturer's instructions.

Immunohistochemistry

For histological identification of BM vessels, frozen BM sections were prepared and immunostained according to the Kawamoto method[93]. Frozen BM sections were fixed in 4% PFA/PBS for 5 min, and washed three times with PBS. After blocking with Protein Block (Dako), BM sections were incubated with primary antibodies for 16 h. Stained specimens were washed three times with PBS and stained with DAPI and fluorophore-labeled secondary antibodies for 4 h at room temperature. All antibodies were diluted in Protein Block (Dako).

To compare the distance of HSPC to sinusoid between young and old mice, whole-mount tissue preparation, immunofluorescence staining, and imaging of the femur were performed as previously described, with slight modifications[94]. Briefly, fleshly isolated young and old Evi1-GFP mouse femurs were immersed in 4% paraformaldehyde (PFA)/phosphate-buffered saline (PBS) for 16 h at 4 °C. Then, specimens were dehydrated in 30% sucrose for 72 h at 4 °C. Next, specimens were embedded in an optimal cutting temperature embedding medium and frozen in liquid nitrogen for 10 min. Specimens were preserved at −80 °C until sectioning. Specimens were repeatedly sectioned with a cryostat until the surface of the BM was fully exposed along the longitudinal axis for femurs. Then, specimens were turned over, and the same sectioning procedure was repeated on the opposite side. After the entire BM sections were generated, sections were washed three times with PBS. Then, they were incubated for 1 h in a blocking solution consisting of 2% bovine serum albumin (BSA), 10% donkey serum, and 0.2% PBS containing Tween (PBST). Next, sections were stained with primary antibodies for 16 h at 4 °C. Then, they were washed 10 times with 0.2% PBST for an hour and stained with DAPI and fluorophore-labeled secondary antibodies for 16 h at 4 °C. Sections were subsequently washed 10 times with 0.2% PBST for 1 h and incubated in RapiClear 1.52 for 16 h. All primary antibodies were diluted in 2% BSA, 10% donkey serum, and 0.2% PBST. All secondary antibodies were diluted in 10% donkey serum and 0.2% PBST. Immunofluorescence data were obtained and analyzed with a confocal laser scanning microscope (LSM880; Zeiss). Distances from HSPCs and random dots to sinusoids were measured using Imaris 9.8.2 software (Oxford Instruments).

Intravital microscopy

Mice were anesthetized by intraperitoneal injection of urethane (800 mg kg^{-1}) and α-chloralose (80 mg kg^{-1}), tracheotomized, and intubated with a handmade Y-shaped tube for mechanical ventilation. The left femoral artery and vein were cannulated for measuring arterial blood pressure and chemical injection. An arterial catheter was connected to a pressure transducer (MP 150; BioPac Systems) to monitor mean arterial pressure continuously. Rectal temperature was maintained at 37.0 ± 0.5 °C throughout the experiment with a heating pad. Animals were mechanically ventilated with a small-animal ventilator

(MiniVent type 845; Harvard Apparatus) with 21% O_2 balanced by N_2 at a tidal volume of 8 μL g^{-1} with a respiratory rate of 120 respirations min^{-1}.

The tibial cortex was planned with a sterilized precision grinder (TAKAGI) to prepare the observation window. Intravital staining with Alexa Fluor 633 (AF633) and acetylated low-density lipoproteins (AcLDLs) were used to identify arteries and sinusoids in BM, respectively[38]. Images were acquired with an FVMPE-RS multiphoton microscope (Evident). Vascular diameter, RBC velocity, and RBC density were measured with multi-photon microscopy as described previously[15,37,38]. Briefly, to visualize calvarial BM microvasculature and to measure vessel diameters, 5 mg of TRITC conjugated-dextran (Sigma) were injected into the femoral vein of an anesthetized mouse. RBC velocity and density were measured by multi-photon microscopy in line-scan mode. These measured parameters were used to calculate RBC flux, blood viscosity, shear rate, and shear stress by a calculation method, as previously reported[15]. Reactivity of blood vessels was demonstrated as a percentage of change in vessel diameter after transcalvarial administration of chemicals, as described previously[38].

For intravital NO imaging, diaminofluorescein-FM diacetate (Goryo chemical, 15 g/kg body weight) was injected via the femoral vein 30 min before fluorescent intensity measurement.

For evaluation of time required for transendothelial migration of HSPC, Lineage-, c-Kit$^+$ (LK) cells obtained from Ubc-GFP mouse BM were injected intravenously. The time period between transplanted LK cell adhesion to calvarial BM endothelial cells and extravasation was measured as the time required for transendothelial migration of an HSPC using the FVMPE-RS multiphoton microscope.

Vascular lumen segmentation was performed using a binary image obtained from higher magnification in vivo fluorescence imaging of the vasculature than previous studies[95–98] to increase the accuracy of vessel recognition, and the vessel/BM volume ratio was analogous by Delesse's principle[99].

RNA isolation and qPCR

RNA-easy mini kit (Cat # 74106, Qiagen) was used for RNA isolation. Reverse transcription was performed using a SuperScript VILO cDNA Synthesis Kit (Cat # 11754050, Invitrogen) SYBR Premix ExTaq IIa (TaKaRa Bio) was used for qPCR according to the manufacturer's instructions. Primers for Chrna1 (forward:5′-GTGGCCATTAACCCGGA AAGT-3′, reverse:5′- CACGGTCAGGGACAGTAAGACA-3′), Chrna2 (forward:5′- CGGTGGCTGATGATGAATCG-3′, reverse:5′-TGCTTTCTGTAT TTGAGGTGACA-3′), Chrna3 (forward:5′- CGTGCTAGCTTAGCTGTGC TT-3′, reverse:5′-GCTTGTAGTCATTCCAGATTTGCTT-3′), Chrna4 (forward:5′-GCCTCTTGCCTGCTAGCA-3′, reverse:5′- CAGGCCTCCAGATG AGTTCA-3′), Chrna5 (forward:5′-GAGCAAGGGGAACCGGAC-3′, reverse:5′- CGCCATAGCATTGTGTGTGGAA-3′), Chrna6 (forward:5′- GG CCAATGTGGATGAAGTCAAC-3′, reverse:5′-TGATGGTCAAACGGGAAG AAG-3′), Chrna7 (forward:5′- ATTCCGTGCCCTTGATAGC-3′, reverse:5′- GGAAGCGGTTGGCGATGTA-3′), Chrna9 (forward:5′-CTTGCGTCCTCA TATCGTTC-3′, reverse:5′-TGCTTTCAGGTTGGACCC-3′), Chrna10 (forward:5′-TGCCTATGTGTGCAACCTACTG-3′, reverse:5′- CGAGCCCAGG CAGGTACTG-3′), Chrnb1 (forward:5′-ACGTTGCCCTGGACATCAAT-3′, reverse:5′-GATCCCCTGGAAGTTGGATT-3′), Chrnb2 (forward:5′- TGGA GCATCTCTTGGATCCTT-3′, reverse:5′-TGGTCAAATGGGAAGTGCTT-3′), Chrnb3 (forward:5′-AATGTGTCCGCCCTGTGTTG-3′, reverse:5′-TGA CGGTTCCGCTGGATTTC-3′), Chrnb4 (forward:5′-TCCGCCTGGAGCT ATCACTGT-3′, reverse:5′- GCGAAATTTGAGGGTGCAGTT-3′), Chrng (forward:5′- GTGCCACTCATCAGCAAGTACCT-3′, reverse:5′-GCTTCA GGCTGCCACAGAAC-3′), Chrnd (forward:5′- GGCAGAACTGCTCCC TCAAA-3′, reverse:5′-GACACAGATCACCACCACCAT-3′), Chrne (forward:5′-CAAGGACGATTTTGCAGGTGTA-3′, reverse:5′-CGGCGGATGAT GAGCGTATA-3′), Chrm1 (forward:5′- CCCCTCTCCGGTCCCAT-3′, reverse:5′- ACGGTGATGTTGGGACTGAC-3′), Chrm2 (forward:5′- CGCT

CCCAAACCGGTCC-3′, reverse:5′- TGTGTTCAGTAGTCAAGTGGC-3′), Chrm3 (forward:5′-CTGGACAGTCCGGGAGATTC-3′, reverse:5′- TCCAC AGTCCACTGAGCAAG-3′), Chrm4 (forward:5′-GCTAGTTCCGCCGTC TGTCC-3′, reverse:5′-AGGCGCACAGACTGATTGG-3′), Chrm5 (forward:5′- TCCTGGTCATCCTCCCGTAG-3′, reverse:5′- TCAGCCTTTTCC CAGTCAGC-3′), eNOS (forward:5′-CCTTCCGCTACCAGCCAGA-3′, reverse:5′-CAGAGATCTTCACTGCATTGGCTA-3′)[100], Piezo1 (forward:5′-ACGTCTACGCCCTCATGTTC-3′, reverse:5′-TGACAGCGAGGATGCA ATGT-3′) and Gapdh (forward:5′-AAATGGTGAAGGTCGTGTG-3′, reverse:5′-TGAAGGGGTCGTTGATGG-3′) were used to quantify target genes. Gene expression was assessed with an ABI 7500 Fast Real-Time PCR System (Applied Biosystems)

Protein level, gene expression, and enzyme activity of AChE

AChE protein levels were determined by Western blot analysis. Mouse femoral and tibial BM was flushed and homogenized in 0.3 mL ice-cold LIPA buffer. Thirty μg of total protein were diluted in Laemmli buffer containing 5% β-mercaptoethanol, denatured for 5 min at 95 °C, separated by SDS/PAGE, and transferred onto PVDF membranes. Membranes were treated in PBS with 0.05% Tween 20 and 5% nonfat milk for 1 h and then incubated overnight at 4 °C with primary antibodies. Membranes were then rinsed with PBS containing Tween 20 and incubated with the HRP-conjugated secondary antibody for 1 h at room temperature. Proteins were detected with ECL reagent (Millipore) using a Lumino image analyzer (LAS4010, GE Healthcare). Protein expression was assessed with Fiji software (ImageJ; National Institutes of Health, NIH). Uncropped and unprocessed scans of the blots are available within the Source Data file.

Gene expression of AChE in BM cells of young and old mice was analyzed by microfluidic droplet-based scRNA-seq data of Tabula Muris Senis (https://tabula-muris-senis.ds.czbiohub.org/). BM data in Tabula Muris Senis were processed using a scRNA-seq data visualization tool cellxgene[101] (https://tabula-muris-senis.ds.czbiohub.org/marrow/droplet/). Data from 1- and 3 month-old mice were used as data of young mice. We also used data of 24- and 30 month-old mice in Tabula Muris Senis for old mouse data.

The enzymatic activity of AChE in BM was evaluated with an Amplite™ Colorimetric Acetylcholinesterase Assay Kit (AAT Bioquest) according to the manufacturer's instructions.

Reanalysis of deposited single-cell RNA-seq data

Single-cell RNA sequencing data (GSE255019)[102] were analyzed using Seurat (v5.1.0) and classified into 11 cell types: HSC, short-term HSC, MPP, MEP, MkP, Erythroid, GMP, monocyte, dendritic cell, neutrophil, and mast cell. Clusters identified by Seurat's FindClusters function were manually annotated based on marker genes detected by FindAllMarkers. Statistical comparisons were conducted using unpaired two-tailed t-tests with the t.test function in R.

BM homing assay

Whole BM mononuclear cells (BMMNCs, 5×10^6 cells) obtained from Ubc-GFP mice were administered intravenously to recipient mice[103]. By using flow cytometry, the ratio of GFP$^+$ HSPC in total recipient BMMNCs obtained from one leg to administrated GFP$^+$ HSPC was evaluated 16 h after BMT as homing efficiency of HSPCs. In the homing assay using old mice, the ratio of GFP$^+$ HSPC in 1×10^7 recipient BMMNCs to administrated GFP$^+$ HSPCs was evaluated as homing efficiency of HSPCs. Yoda1 was administered intravenously (0.5 μmol/kg body weight) just after BMT[104]. For Piezo1 inhibition, GdCl$_3$ was administered subcutaneously (40 mg/kg body weight) just before BMT[104].

Evaluation of hematopoietic reconstitution after myelosuppression

Mice received 9.0 Gy irradiation as a lethal, low-skin damaging, low-gastrointestinal damaging dose, followed by i.v. administration of 1×10^5 whole BM cells (BMT). Retro-orbital peripheral blood was collected using a calibrated pipet (Drummond) every 2 or 3 days after transplantation. WBC counts, RBC counts, and platelets numbers were obtained using Celltac α hematology analyzer (Nihon Khoden)[8].

HSC transplantation

A total of 500 HSCs from young mice (Ly5.1) were transplanted into lethally-irradiated (9.0 Gy) young or middle-aged recipients (Ly5.2). Yoda1 (0.5 μmol/kg body weight) or DMSO was injected into the retro-orbital plexus of recipients 0, 2, and 4 h after HSCT. After 24 h after HSCT, 1×10^6 BMMNCs (Ly5.2) were transplanted into them. Donor chimerism was detected by flow cytometry 4, 8, and 12 weeks after HSCT.

Statistical analysis

All values presented here are expressed as means ± SEM unless noted otherwise. Differences between means were evaluated for significance using Two-sided Student's t-test unless specified otherwise. For survival curves, statistical analysis was performed with the log-rank (Mantel–Cox) test. Differences with a p-value < 0.05 were considered statistically significant.

Illustrations

The illustrations in Fig. 1a, Fig. 3a, Fig. 5g, Fig. 6a, Fig. 7a, f, i, k, Supplementary Fig. 8a, Supplementary Fig. 15e were created by T Morikawa using Inkscape. We do not use any third-party drawing material in this manuscript.

Reporting summary

Further information on research design is available in the Nature Portfolio Reporting Summary linked to this article.

Data availability

The main data supporting the results of this study are presented in the paper and its supplemental figures. Details of the data sets and protocols supporting the results of this study will be provided by the corresponding author upon request. Source data are provided with this paper.

References

1. Hoggatt, J., Kfoury, Y. & Scadden, D. T. Hematopoietic stem cell niche in health and disease. *Annu Rev. Pathol.* **11**, 555–581 (2016).
2. Comazzetto, S., Shen, B. & Morrison, S. J. Niches that regulate stem cells and hematopoiesis in adult bone marrow. *Dev. Cell* **56**, 1848–1860 (2021).
3. Pinho, S. & Frenette, P. S. Haematopoietic stem cell activity and interactions with the niche. *Nat. Rev. Mol. Cell Biol.* **20**, 303–320 (2019).
4. Ho, Y. H. & Méndez-Ferrer, S. Microenvironmental contributions to hematopoietic stem cell aging. *Haematologica* **105**, 38–46 (2020).
5. Wright, D. E., Wagers, A. J., Gulati, A. P., Johnson, F. L. & Weissman, I. L. Physiological migration of hematopoietic stem and progenitor cells. *Science* **294**, 1933–1936 (2001).
6. Schwarz, B. A. & Bhandoola, A. Circulating hematopoietic progenitors with T lineage potential. *Nat. Immunol.* **5**, 953–960 (2004).
7. Massberg, S. et al. Immunosurveillance by hematopoietic progenitor cells trafficking through blood, lymph, and peripheral tissues. *Cell* **131**, 994–1008 (2007).
8. Liang, Y., Van Zant, G. & Szilvassy, S. J. Effects of aging on the homing and engraftment of murine hematopoietic stem and progenitor cells. *Blood* **106**, 1479–1487 (2005).
9. Marenzana, M. & Arnett, T. R. The key role of the blood supply to bone. *Bone Res.* **1**, 203–215 (2013).

10. Itkin, T. et al. Distinct bone marrow blood vessels differentially regulate haematopoiesis. *Nature* **532**, 323–328 (2016).

11. Sipkins, D. A. et al. In vivo imaging of specialized bone marrow endothelial microdomains for tumour engraftment. *Nature* **435**, 969–973 (2005).

12. Lo Celso, C. et al. Live-animal tracking of individual haematopoietic stem/progenitor cells in their niche. *Nature* **457**, 92–96 (2009).

13. Heazlewood, S. Y., Oteiza, A., Cao, H. & Nilsson, S. K. Analyzing hematopoietic stem cell homing, lodgment, and engraftment to better understand the bone marrow niche. *Ann. N. Y Acad. Sci.* **1310**, 119–128 (2014).

14. Nourshargh, S. & Alon, R. Leukocyte migration into inflamed tissues. *Immunity* **41**, 694–707 (2014).

15. Bixel, M. G. et al. Flow dynamics and HSPC homing in bone marrow microvessels. *Cell Rep.* **18**, 1804–1816 (2017).

16. Ponomaryov, T. et al. Induction of the chemokine stromal-derived factor-1 following DNA damage improves human stem cell function. *J. Clin. Invest* **106**, 1331–1339 (2000).

17. Ara, T. et al. Long-term hematopoietic stem cells require stromal cell-derived factor-1 for colonizing bone marrow during ontogeny. *Immunity* **19**, 257–267 (2003).

18. Hoggatt, J., Singh, P., Sampath, J. & Pelus, L. M. Prostaglandin E2 enhances hematopoietic stem cell homing, survival, and proliferation. *Blood* **113**, 5444–5455 (2009).

19. Grassinger, J. et al. Thrombin-cleaved osteopontin regulates hemopoietic stem and progenitor cell functions through interactions with alpha9beta1 and alpha4beta1 integrins. *Blood* **114**, 49–59 (2009).

20. Kimura, T. et al. The sphingosine 1-phosphate receptor agonist FTY720 supports CXCR4-dependent migration and bone marrow homing of human CD34+ progenitor cells. *Blood* **103**, 4478–4486 (2004).

21. Gu, Y. et al. Hematopoietic cell regulation by Rac1 and Rac2 guanosine triphosphatases. *Science* **302**, 445–449 (2003).

22. Potocnik, A. J., Brakebusch, C. & Fässler, R. Fetal and adult hematopoietic stem cells require beta1 integrin function for colonizing fetal liver, spleen, and bone marrow. *Immunity* **12**, 653–663 (2000).

23. Scott, L. M., Priestley, G. V. & Papayannopoulou, T. Deletion of alpha4 integrins from adult hematopoietic cells reveals roles in homeostasis, regeneration, and homing. *Mol. Cell Biol.* **23**, 9349–9360 (2003).

24. Vermeulen, M. et al. Role of adhesion molecules in the homing and mobilization of murine hematopoietic stem and progenitor cells. *Blood* **92**, 894–900 (1998).

25. Papayannopoulou, T., Craddock, C., Nakamoto, B., Priestley, G. V. & Wolf, N. S. The VLA4/VCAM-1 adhesion pathway defines contrasting mechanisms of lodgement of transplanted murine hemopoietic progenitors between bone marrow and spleen. *Proc. Natl. Acad. Sci. USA* **92**, 9647–9651 (1995).

26. Frenette, P. S., Subbarao, S., Mazo, I. B., von Andrian, U. H. & Wagner, D. D. Endothelial selectins and vascular cell adhesion molecule-1 promote hematopoietic progenitor homing to bone marrow. *Proc. Natl. Acad. Sci. USA* **95**, 14423–14428 (1998).

27. Katayama, Y. et al. PSGL-1 participates in E-selectin-mediated progenitor homing to bone marrow: evidence for cooperation between E-selectin ligands and alpha4 integrin. *Blood* **102**, 2060–2067 (2003).

28. Murakami, J. L. et al. Evidence that β7 Integrin Regulates Hematopoietic Stem Cell Homing and Engraftment Through Interaction with MAdCAM-1. *Stem Cells Dev.* **25**, 18–26 (2016).

29. Ruppert, R. et al. Kindlin-3-mediated integrin adhesion is dispensable for quiescent but essential for activated hematopoietic stem cells. *J. Exp. Med.* **212**, 1415–1432 (2015).

30. Mei, Y. et al. Diaphanous-related formin mDia2 regulates beta2 integrins to control hematopoietic stem and progenitor cell engraftment. *Nat. Commun.* **11**, 3172 (2020).

31. Avigdor, A. et al. CD44 and hyaluronic acid cooperate with SDF-1 in the trafficking of human CD34+ stem/progenitor cells to bone marrow. *Blood* **103**, 2981–2989 (2004).

32. Cinamon, G., Shinder, V. & Alon, R. Shear forces promote lymphocyte migration across vascular endothelium bearing apical chemokines. *Nat. Immunol.* **2**, 515–522 (2001).

33. Wang, S. et al. Mechanosensation by endothelial PIEZO1 is required for leukocyte diapedesis. *Blood* **140**, 171–183 (2022).

34. Chandel N. S. Mitochondria. *Cold Spring Harb Perspect Biol.* **13**, a040543 (2021).

35. Atkinson, D. E. The energy charge of the adenylate pool as a regulatory parameter. Interaction with feedback modifiers. *Biochemistry* **7**, 4030–4034 (1968).

36. Kataoka, K. et al. Evi1 is essential for hematopoietic stem cell self-renewal, and its expression marks hematopoietic cells with long-term multilineage repopulating activity. *J. Exp. Med.* **208**, 2403–2416 (2011).

37. Morikawa, T. et al. Hypoxic regulation of the cerebral microcirculation is mediated by a carbon monoxide-sensitive hydrogen sulfide pathway. *Proc. Natl. Acad. Sci. USA* **109**, 1293–1298 (2012).

38. Morikawa, T., Tamaki, S., Fujita, S., Suematsu, M. & Takubo, K. Identification and local manipulation of bone marrow vasculature during intravital imaging. *Sci. Rep.* **10**, 6422 (2020).

39. Furchgott, R. F. & Zawadzki, J. V. The obligatory role of endothelial cells in the relaxation of arterial smooth muscle by acetylcholine. *Nature* **288**, 373–376 (1980).

40. Dykstra, B., Olthof, S., Schreuder, J., Ritsema, M. & de Haan, G. Clonal analysis reveals multiple functional defects of aged murine hematopoietic stem cells. *J. Exp. Med.* **208**, 2691–2703 (2011).

41. Sudo, K., Ema, H., Morita, Y. & Nakauchi, H. Age-associated characteristics of murine hematopoietic stem cells. *J. Exp. Med.* **192**, 1273–1280 (2000).

42. Mansell, E. et al. Mitochondrial potentiation ameliorates age-related heterogeneity in hematopoietic stem cell function. *Cell Stem Cell* **28**, 241–256.e246 (2021).

43. Fujii, T. et al. Physiological functions of the cholinergic system in immune cells. *J. Pharm. Sci.* **134**, 1–21 (2017).

44. Tallini, Y. N. et al. BAC transgenic mice express enhanced green fluorescent protein in central and peripheral cholinergic neurons. *Physiol. Genomics* **27**, 391–397 (2006).

45. Reardon, C. et al. Lymphocyte-derived ACh regulates local innate but not adaptive immunity. *Proc. Natl. Acad. Sci. USA* **110**, 1410–1415 (2013).

46. Schloss, M. J. et al. B lymphocyte-derived acetylcholine limits steady-state and emergency hematopoiesis. *Nat. Immunol.* **23**, 605–618 (2022).

47. Soreq, H. & Seidman, S. Acetylcholinesterase-new roles for an old actor. *Nat. Rev. Neurosci.* **2**, 294–302 (2001).

48. Lee, J. & Cooke, J. P. Nicotine and pathological angiogenesis. *Life Sci.* **91**, 1058–1064 (2012).

49. Nakamura, T. et al. M(3) muscarinic acetylcholine receptor plays a critical role in parasympathetic control of salivation in mice. *J. Physiol.* **558**, 561–575 (2004).

50. Kuribayashi W. et al. Limited rejuvenation of aged hematopoietic stem cells in young bone marrow niche. *J. Exp. Med.* **218**, e20192283 (2021).

51. Ho T. T. et al. Aged hematopoietic stem cells are refractory to bloodborne systemic rejuvenation interventions. *J. Exp. Med.* **218**, e20210223 (2021).

52. Fares, I. et al. Cord blood expansion. Pyrimidoindole derivatives are agonists of human hematopoietic stem cell self-renewal. *Science* **345**, 1509–1512 (2014).

53. Wilkinson, A. C. et al. Long-term ex vivo haematopoietic-stem-cell expansion allows nonconditioned transplantation. *Nature* **571**, 117–121 (2019).

54. Sakurai, M. et al. Chemically defined cytokine-free expansion of human haematopoietic stem cells. *Nature* **615**, 127–133 (2023).

55. Speth, J. M., Hoggatt, J., Singh, P. & Pelus, L. M. Pharmacologic increase in HIF1α enhances hematopoietic stem and progenitor homing and engraftment. *Blood* **123**, 203–207 (2014).

56. Grüneboom, A. et al. A network of trans-cortical capillaries as mainstay for blood circulation in long bones. *Nat. Metab.* **1**, 236–250 (2019).

57. Dahlmann, B. Role of proteasomes in disease. *BMC Biochem.* **8**, S3 (2007).

58. Dellorusso, P. V. et al. Autophagy counters inflammation-driven glycolytic impairment in aging hematopoietic stem cells. *Cell Stem Cell* **31**, 1020–1037.e1029 (2024).

59. Watanuki, S. et al. SDHAF1 confers metabolic resilience to aging hematopoietic stem cells by promoting mitochondrial ATP production. *Cell Stem Cell* **31**, 1145–1161.e1115 (2024).

60. Nikolaou, C. et al. High-dimensional single cell mass cytometry analysis of the murine hematopoietic system reveals signatures induced by ageing and physiological pathogen challenges. *Immun. Ageing* **18**, 20 (2021).

61. van Beek, A. A. et al. Aged mice display altered numbers and phenotype of basophils, and bone marrow-derived basophil activation, with a limited role for aging-associated microbiota. *Immun. Ageing* **15**, 32 (2018).

62. Gekas, C. & Graf, T. CD41 expression marks myeloid-biased adult hematopoietic stem cells and increases with age. *Blood* **121**, 4463–4472 (2013).

63. Connor, K. M. et al. Understanding metabolic changes in aging bone marrow. *Exp. Hematol. Oncol.* **7**, 13 (2018).

64. Zhang, C. et al. Sex-dependent differences in hematopoietic stem cell aging and leukemogenic potential. *Oncogene* **44**, 64–78 (2025).

65. Rodriguez, S. et al. Dysfunctional expansion of hematopoietic stem cells and block of myeloid differentiation in lethal sepsis. *Blood* **114**, 4064–4076 (2009).

66. Gupta, V. et al. Impact of age on outcomes after bone marrow transplantation for acquired aplastic anemia using HLA-matched sibling donors. *Haematologica* **95**, 2119–2125 (2010).

67. Kusumbe, A. P. et al. Age-dependent modulation of vascular niches for haematopoietic stem cells. *Nature* **532**, 380–384 (2016).

68. Gur-Cohen, S. et al. PAR1 signaling regulates the retention and recruitment of EPCR-expressing bone marrow hematopoietic stem cells. *Nat. Med.* **21**, 1307–1317 (2015).

69. Nevo, N. et al. Enhanced thrombin/PAR1 activity promotes G-CSF- and AMD3100-induced mobilization of hematopoietic stem and progenitor cells via NO upregulation. *Leukemia* **35**, 3334–3338 (2021).

70. Furuhashi, K. et al. Bone marrow niches orchestrate stem-cell hierarchy and immune tolerance. *Nature* **638**, 206–215 (2025).

71. Liu, H. Rosen C. J. Nitric oxide and bone: the phoenix rises again. *J. Clin. Invest.* **131**, e147072 (2021).

72. Jin, Z. et al. Nitric oxide modulates bone anabolism through regulation of osteoblast glycolysis and differentiation. *J. Clin. Invest.* **131**, e138935 (2021).

73. Asada, N. & Katayama, Y. Regulation of hematopoiesis in endosteal microenvironments. *Int. J. Hematol.* **99**, 679–684 (2014).

74. Michurina, T. et al. Nitric oxide is a regulator of hematopoietic stem cell activity. *Mol. Ther.* **10**, 241–248 (2004).

75. Kollet, O. et al. Osteoclasts degrade endosteal components and promote mobilization of hematopoietic progenitor cells. *Nat. Med.* **12**, 657–664 (2006).

76. Thomas, D. D., Liu, X., Kantrow, S. P. & Lancaster, J. R. Jr The biological lifetime of nitric oxide: implications for the perivascular dynamics of NO and O_2. *Proc. Natl. Acad. Sci. USA* **98**, 355–360 (2001).

77. Katayama, Y. et al. Signals from the sympathetic nervous system regulate hematopoietic stem cell egress from bone marrow. *Cell* **124**, 407–421 (2006).

78. Hanoun, M., Maryanovich, M., Arnal-Estapé, A. & Frenette, P. S. Neural regulation of hematopoiesis, inflammation, and cancer. *Neuron* **86**, 360–373 (2015).

79. Pierce, H. et al. Cholinergic signals from the CNS regulate G-CSF-mediated HSC mobilization from bone marrow via a glucocorticoid signaling relay. *Cell Stem Cell* **20**, 648–658.e644 (2017).

80. Spiegel, A. et al. Catecholaminergic neurotransmitters regulate migration and repopulation of immature human CD34+ cells through Wnt signaling. *Nat. Immunol.* **8**, 1123–1131 (2007).

81. Spiegel, A., Kalinkovich, A., Shivtiel, S., Kollet, O. & Lapidot, T. Stem cell regulation via dynamic interactions of the nervous and immune systems with the microenvironment. *Cell Stem Cell* **3**, 484–492 (2008).

82. Fielding, C. et al. Cholinergic signals preserve haematopoietic stem cell quiescence during regenerative haematopoiesis. *Nat. Commun.* **13**, 543 (2022).

83. Yamada, M. et al. Cholinergic dilation of cerebral blood vessels is abolished in M(5) muscarinic acetylcholine receptor knockout mice. *Proc. Natl. Acad. Sci. USA* **98**, 14096–14101 (2001).

84. Takahashi, T. et al. Non-neuronal acetylcholine as an endogenous regulator of proliferation and differentiation of Lgr5-positive stem cells in mice. *Febs J.* **281**, 4672–4690 (2014).

85. Sastry, B. V. & Sadavongvivad, C. Cholinergic systems in non-nervous tissues. *Pharm. Rev.* **30**, 65–132 (1978).

86. Horiuchi, Y. et al. Evolutional study on acetylcholine expression. *Life Sci.* **72**, 1745–1756 (2003).

87. Wessler, I., Kilbinger, H., Bittinger, F. & Kirkpatrick, C. J. The biological role of non-neuronal acetylcholine in plants and humans. *Jpn J. Pharm.* **85**, 2–10 (2001).

88. Huang, P. L. et al. Hypertension in mice lacking the gene for endothelial nitric oxide synthase. *Nature* **377**, 239–242 (1995).

89. Takubo, K. et al. Regulation of glycolysis by Pdk functions as a metabolic checkpoint for cell cycle quiescence in hematopoietic stem cells. *Cell Stem Cell* **12**, 49–61 (2013).

90. Pietras, E. M. et al. Functionally distinct subsets of lineage-biased multipotent progenitors control blood production in normal and regenerative conditions. *Cell Stem Cell* **17**, 35–46 (2015).

91. Xu, C. et al. Stem cell factor is selectively secreted by arterial endothelial cells in bone marrow. *Nat. Commun.* **9**, 2449 (2018).

92. Karigane, D. et al. p38α activates purine metabolism to initiate hematopoietic stem/progenitor cell cycling in response to stress. *Cell Stem Cell* **19**, 192–204 (2016).

93. Kawamoto, T. Use of a new adhesive film for the preparation of multi-purpose fresh-frozen sections from hard tissues, whole-animals, insects and plants. *Arch. Histol. Cytol.* **66**, 123–143 (2003).

94. Fujita, S. et al. Quantitative analysis of sympathetic and nociceptive innervation across bone marrow regions in mice. *Exp. Hematol.* **112-113**, 44–59.e46 (2022).

95. Kunisaki, Y. et al. Arteriolar niches maintain haematopoietic stem cell quiescence. *Nature* **502**, 637–643 (2013).

96. Gomariz, A. et al. Quantitative spatial analysis of haematopoiesis-regulating stromal cells in the bone marrow microenvironment by 3D microscopy. *Nat. Commun.* **9**, 2532 (2018).

97. Vandoorne, K. et al. Imaging the vascular bone marrow niche during inflammatory stress. *Circ. Res.* **123**, 415–427 (2018).

98. Lee, K. et al. Ultralow-dose irradiation enables engraftment and intravital tracking of disease initiating niches in clonal hematopoiesis. *Sci. Rep.* **14**, 20486 (2024).

99. St Pierre, T. G. et al. Stereological analysis of liver biopsy histology sections as a reference standard for validating non-invasive liver fat fraction measurements by MRI. *PLoS One* **11**, e0160789 (2016).

100. Passaro, D. et al. Increased vascular permeability in the bone marrow microenvironment contributes to disease progression and drug response in acute Myeloid Leukemia. *Cancer Cell* **32**, 324–341.e326 (2017).

101. Megill, C. et al. cellxgene: a performant, scalable exploration platform for high dimensional sparse matrices. *bioRxiv* https://doi.org/10.1101/2021.04.05.438318 (2021).

102. Poscablo, D. M. et al. An age-progressive platelet differentiation path from hematopoietic stem cells causes exacerbated thrombosis. *Cell* **187**, 3090–3107.e3021 (2024).

103. Takubo, K. et al. Regulation of the HIF-1alpha level is essential for hematopoietic stem cells. *Cell Stem Cell* **7**, 391–402 (2010).

104. Atcha, H. et al. Mechanically activated ion channel Piezo1 modulates macrophage polarization and stiffness sensing. *Nat. Commun.* **12**, 3256 (2021).

Acknowledgements

Author contributions

T.Mo., S.F., Y.S., S.T., M.H., K.S., S.W., H.K., H.K.-S., Y.N., N.H., T.Ma., and T.H. performed the study and analyzed data. M.M., M.T., and M.S. provided scientific advice and materials; T.Mo. and K.T. wrote the manuscript; and K.T. conceived the project and supervised the research.

Competing interests

The authors declare no competing interests.

Additional information